Basin and Petroleum System Modeling
7th Annual Industrial Affiliates Meeting
and
Field Trip to Black Diamond Mines Regional Preserve

November 11-13, 2014
Stanford, California

Compiled by Allegra Hosford Scheirer,
Les Magoon, and Steve Graham
http://bpsm.stanford.edu

2014 BPSM Industrial Affiliates

Aera Energy LLC
BP
Chevron
ConocoPhillips
Great Bear Petroleum LLC
Hess Corporation
Murphy Exploration & Production Co (new for 2014)
Nexen Petroleum Inc.
Oxy
PEMEX (new for 2015)
Petrobras
Saudi Aramco
Schlumberger

Schedule of Events

- Tuesday, 11/11/14, 5:30-7:30pm Icebreaker at Stanford Golf Course
- Wednesday, 11/12/14, 9am-5pm Oral Session at Oak West in Tresidder Memorial Union, followed by group dinner at 6:30pm at Gravity Wine Bar, Palo Alto
- Thursday, 11/13/14, 2014 8am-4:30pm Field Trip to Black Diamond Mines Regional Preserve

November 12, 2014 Oral Session Agenda

9:00 a.m.	**Steve Graham**, Introduction
9:20 a.m.	**Inessa Yurchenko**, Unraveling hydrocarbon charge history of the Shublik Formation, central North Slope of Alaska
10:00 a.m.	**Mustafa Al Ibrahim**, Integrated Geologic Characterization of Carbonate Mudrocks: The Case of the Tuwaiq Mountain and Hanifa Formations, Saudi Arabia
10:35-10:50 a.m.	Coffee break
10:50 a.m.	**Wisam AlKawai**, Integrating basin modeling with seismic attributes through rock physics
11:15 a.m.	**Lauren Schultz**, Basin and petroleum system modeling in the Los Angeles Basin, California
11:40 a.m.	**Wisam AlKawai**, Investigating the impact of allochthonous salt and overpressure on petroleum system development in the Thunder Horse minibasin by integrating 3D basin and petroleum system modeling with quantitative seismic interpretation
12:10-1:30 p.m.	Lunch (please complete field trip forms if haven't already done so)
1:30 p.m.	**Danica Dralus,** Kinetics of the opal-A to opal-CT phase transition in low- and high-TOC siliceous shale source rocks
2:00 p.m.	**Amrita Sen**, BPSM benchmark basin model project
2:25-2:45 p.m.	Coffee break
2:45 p.m.	**Will Thompson-Butler**, A geochemical assessment of the Utica Shale in the Mohawk Valley of New York
3:15 p.m.	**Tapan Mukerji**, Introductory comments on uncertainty analysis in basin modeling
3:20 p.m.	**Yao Tong**, Basin and petroleum system modeling and sensitivity analysis of Piceance Basin, CO
3:50 p.m.	**Mike Moldowan**, Novel geochemical technologies set the stage for correct models of complex basins
4:20 p.m.	**Ken Peters**, Petroleum generation kinetics: single- versus multiple heating-rate open-system pyrolysis

2014 Meeting Attendees

Attendee	Organization
Lisa Alpert	Aera Energy LLC
José Araujo	Petrobras
Bill DeMis	Southwestern Energy Company
Felix Desperrier	Sonoma State University
Danica Dralus	BP America, Inc. (formerly Stanford)
Ed Duncan	Great Bear Petroleum
Karen Bryant Duncan	Great Bear Petroleum
Carlos Fracalossi	Petrobras
Dave Greeley	BP (by video conference)
Joel Greer	Southwestern Energy Company
Korey Harvey	Oxy
Jie Huang	Hess Corporation
Benjamin Kirkland	Nexen Petroleum
Carolyn Lampe	Ucon Geoconsulting (also at Stanford)
Mike Moldowan	Biomarker Technologies, Inc. (SU Emeritus)
Christophe Mornet	ConocoPhillips
Fausto Mosca	Murphy Exploration & Production
Gary Muscio	Chevron ETC
Kenneth Peters	Schlumberger (also at Stanford)
Gregg Pyke	Occidental Oil & Gas
Stefan Punnette	BP America, Inc.
Constantin Sandu	Chevron
Noelle Schoellkopf	Schlumberger (also at Stanford)
Danny Schwarzer	ConocoPhillips
Ness Shona	Nexen Petroleum

Stanford University Students* and Scientists

Mustafa Al Ibrahim*	Kenneth E. Peters
Wisam AlKawai*	Lauren Schultz*
Steve Graham	Amrita Sen*
Allegra Hosford Scheirer	William Thompson-Butler*
Les Magoon	Yao Tong*
Chven Mitchell*	Inessa Yurchenko*
Tapan Mukerji	

2014 Meeting Abstracts

http://bpsm.stanford.edu

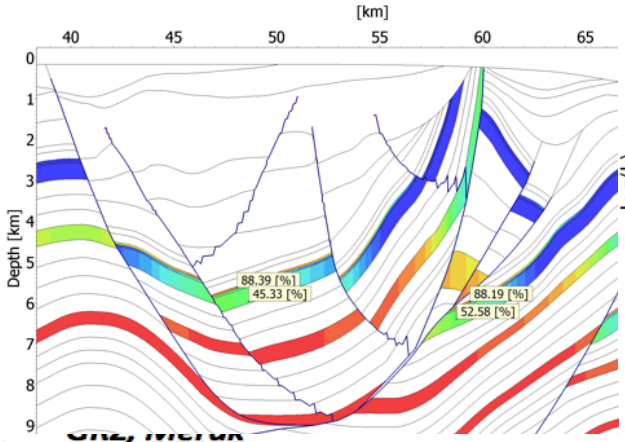

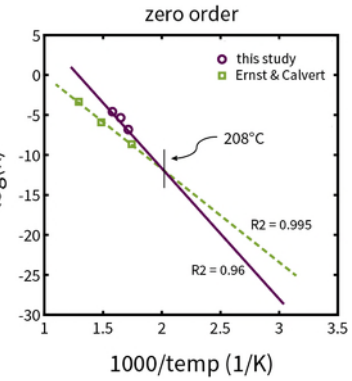

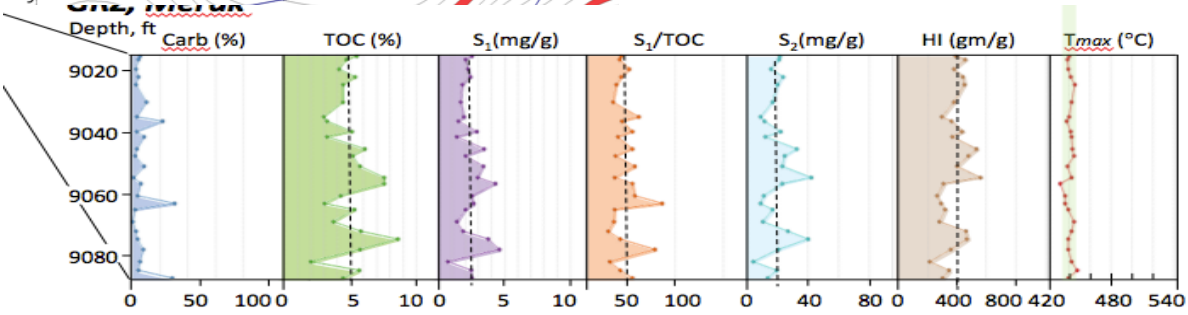

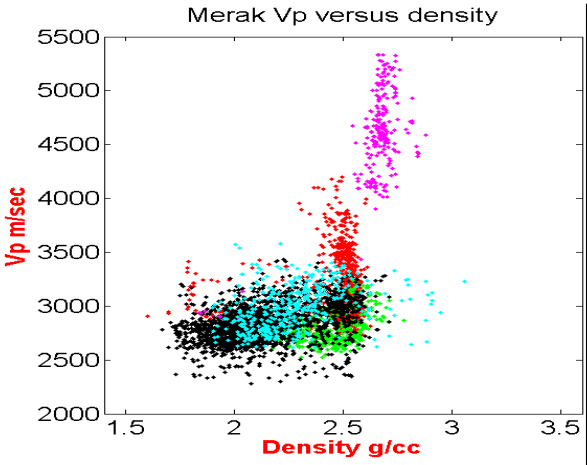

UNRAVELLING HYDROCARBON CHARGE HISTORY OF THE SHUBLIK FORMATION, CENTRAL NORTH SLOPE OF ALASKA

Inessa Yurchenko
Department of Geological and Environmental Sciences, Stanford University

The origin of hydrocarbons in the Central North Slope has been debated and discussed in numerous publications since the discovery of the Prudhoe Bay field in 1967. It has been widely recognized that crude oil accumulations in the North Slope commonly represent a mixture of oils derived from several source rocks (Seifert et al., 1980, Wicks et al., 1991, Masterson, 2001, Peters et al., 2008). The present character of the key petroleum source rocks in the North Slope has only been documented in the most heavily explored regions, however the source rock quality across much of the area remains poorly documented due to limited data (Bird and Houseknecht, 2011).

The Middle to Upper Triassic Shublik Formation is considered to be the major source rock for oil in the North Slope and the greater Prudhoe Bay field area (Fig. 1; Magoon and Bird, 1985; Bird, 2001). Bird (1994) reported that total organic carbon (TOC) of the Shublik ranges from 0.49 to 6.73 wt.% with an average value of 2.3 wt.%. However, the majority of the present day Shublik is mature to overmature, which complicates estimation of the original TOC and source rock generative potential (Peters et al., 2007). Reported Shublik thickness varies from 79 to 489 ft (Bird, 1994).

Shublik Formation is a laterally and vertically heterogeneous unit that has been described both in outcrop and in the subsurface. Parrish (1987) conducted facies analysis of the Shublik Formation in 3 outcrops near the Arctic National Wildlife Refuge (ANWR) and 13 cores from the National Petroleum Reserve of Alaska (NPRA) (Fig. 2). As a result, four distinct lithofacies were described as following: (1) fossiliferous sandstone or siltstone; (2) glauconitic sandstone or siltstone; (3) calcareous mudstone or limestone with phosphate nodules; and (4) black calcareous mudstone or limestone, typically fossiliferous (Parrish, 1987). Kupecz (1995) subdivided Shublik Formation within the Prudhoe Bay field unit into four zones (from A to D) based on their gamma-ray log signature. Hulm (1999) extended this interpretation into the National Petroleum Reserve of Alaska (NPRA) area, and moreover gave a detailed conventional core description for 10 wells that resulted in subdivision of the Shublik Formation into 12 depositional facies (Fig. 2). Kelly et al. (2007) conducted a detail lithologic and geochemical study of the Shublik Formation and the distal equivalent Otuk Formation from three outcrops in order to provide a basis for understanding the lateral and vertical distribution of the various upwelling-related facies (Fig. 2).

Despite this multitude of work, the majority of the Central North Slope remains unexplored. Thus, documentation and high-resolution geochemical and stratigraphic analysis of the Shublik Formation in this region is essential for calculating petroleum charge and testing developed depositional models. This work investigates source rock geochemistry, stratigraphic architecture, and unconventional shale resource analysis of the Shublik Formation in the context of petroleum system modeling.

Figure 1. Generalized stratigraphy of the North Slope of Alaska (Modified from Bird and Houseknecht, 2011).

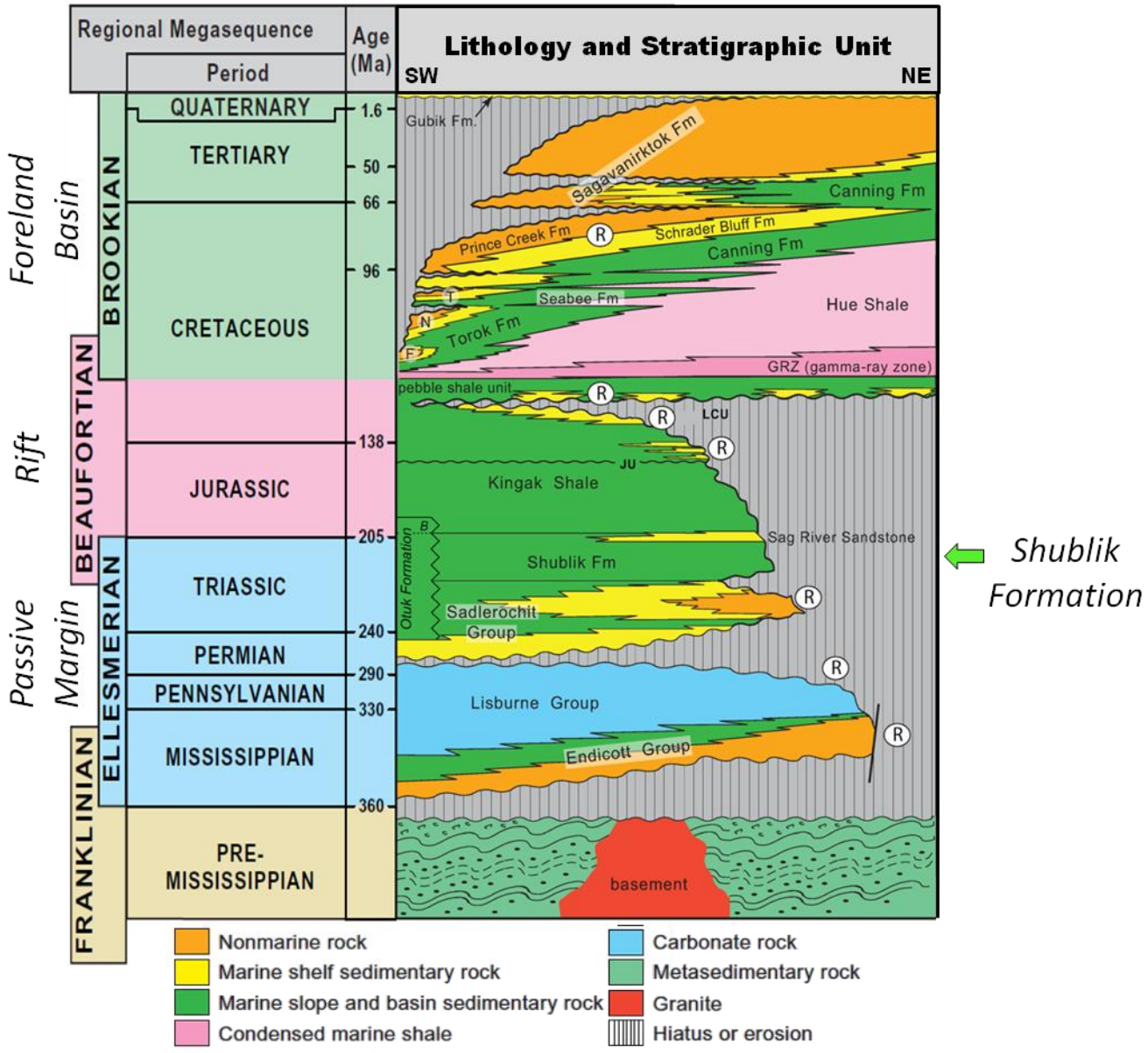

Figure 2. Map of the North Slope of Alaska showing locations of cores and outcrops examined by Parrish et al. (2001), Hulm (1999), Peters et al. (2006), and Kelly et al. (2007). Base map is modified after Parrish et al. (2001).

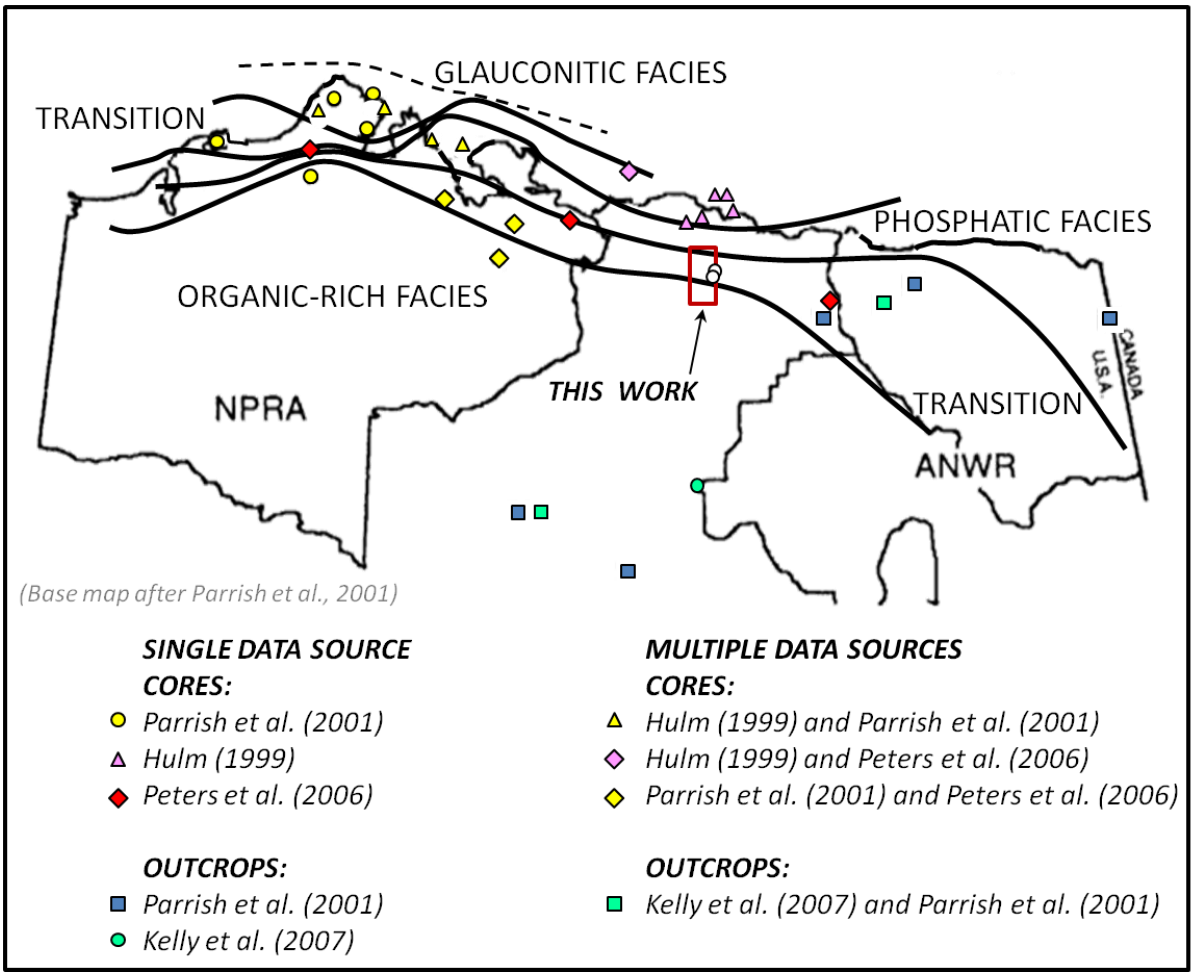

References

Bird, K.J., 1994. Ellesmerian(!) petroleum system, North Slope, Alaska, USA, in Magoon, L.B., Dow, W.G., eds., The Petroleum System – From Source to Trap. Tulsa, AAPG Memoir 60, p. 339–358.

Bird, K. J., 2001, Alaska: A twenty-first-century petroleum province, in M.W. Downey, J. C. Threet, and W. A. Morgan, eds., Petroleum provinces of the twenty-first century: AAPG Memoir 74, p. 137-165.

Bird, K.J., and Houseknecht, D.W., 2011, Geology and petroleum potential of Arctic Alaska, in Spencer, A.M., Embry, A.F., Gautier, D.L., Stoupakova, A.V., and Sørensen, K., eds., Arctic petroleum geology: Geological Society of London Memoir 35, p. 485–499.

Kelly, L.N., Whalen, M.T., McRoberts, C.A., Hopkin, E., and Tomsich, C.S., 2007, Sequence stratigraphy and geochemistry of the upper Lower through Upper Triassic of Northern

Alaska: Implications for paleoredox history, source rock accumulation, and paleoceanography: Alaska Division of Geological & Geophysical Surveys Report of Investigation 2007-1, 50 p.

Kupecz, J.A., 1995, Depositional setting, sequence stratigraphy, diagenesis, and reservoir potential of a mixed-lithology, upwelling deposit, Upper Triassic Shublik Formation, Prudhoe Bay, Alaska: AAPG Bulletin, v. 79, no. 9, p. 1301–1319.

Magoon, L.B. and Bird, K.J., 1985. Alaskan North Slope petroleum geochemistry for the Shublik Formation, Kingak Shale, pebble shale unit, and Torok Formation, in Magoon, L.B., Claypool, G.E., eds., Alaska North Slope Oil/Source Rock Correlation Study, vol. 20. Tulsa, AAPG Studies in Geology, pp. 31–48.

Masterson, W. D., 2001, Petroleum filling history of central Alaskan North Slope fields: Ph.D. thesis, University of Texas at Dallas, Dallas, Texas, 222 p.

Parrish, J.T., 1987, Lithology, geochemistry, and depositional environment of the Triassic Shublik Formation, northern Alaska, in Tailleur, I.L., and Weimer, P., eds., Alaskan North Slope geology: Field Trip Guidebook – SEPM, Pacific Section, Special Publication 50, p. 391–396.

Parrish, J.T., Whalen, M.T., and Hulm, E.J., 2001, Shublik Formation lithofacies, environments, andsequence stratigraphy, Arctic Alaska, U.S.A., in Houseknecht, D.W., ed., Petroleum Plays and Systems in the National Petroleum Reserve – Alaska: SEPM (Society for Sedimentary Geology) Core Workshop No. 21, p. 89–110.

Peters, K.E., Magoon, L.B., Bird, K.J., Valin, Z.C., and Keller, M.A., 2006, North Slope, Alaska: source rock distribution, richness, thermal maturity, and petroleum charge, AAPG Bulletin 90, p. 261–292.

Peters, K. E., Ramos, S. L., Zumberge, J. E., Valin, Z. C., and Bird, K. J., 2008, De-convoluting mixed crude oil in Prudhoe Bay Field, North Slope, Alaska: Organic Geochemistry 39.

Seifert, W. K., Moldowan, J. M., and Jones, R. W., 1980, Application of biological marker chemistry to petroleum exploration: Proceedings of the 10th World Petroleum Congress, Bucharest, Romania, September 1979, Paper SP8: Heyden & Son Inc., Philadelphia, Pennsylvania, p. 425–440.

Wicks, J. L., Buckingham, M. L., and Dupree, J. H., 1991, Endicott field– U.S.A., North Slope basin, Alaska, in N. H. Foster and E. A. Beaumont, eds., Structural traps V: AAPG Treatise of Petroleum Geology, Atlas of Oil and Gas Fields, p. 1–25.

Acknowledgments

Data and funding for this research are generously provided by Great Bear Petroleum LLC. This research has greatly benefited from through collaboration and discussion with my committee members Steve Graham, Tapan Mukerji, Mike Moldowan, Ken Peters, and Allegra Hosford Scheirer, as well as with Les Magoon, Ken Bird, and Carolyn Lampe.

INTEGRATED GEOLOGIC CHARACTERIZATION OF CARBONATE MUDROCKS: THE CASE OF THE TUWAIQ MOUNTAIN AND HANIFA FORMATIONS, SAUDI ARABIA

Mustafa Al Ibrahim[1], Rick Sarg[2], Neil Hurley[3], Dave Cantrell[4], and John Humphrey[2]
[1]*Department of Energy Resources Engineering, Stanford University (formerly Colorado School of Mines)*
[2]*Colorado School of Mines*
[3]*Chevron Technology Company*
[4]*Saudi Aramco*

A proper reservoir characterization requires a grasp of the geologic processes responsible for deposition and diagenesis. Studying carbonate mudrocks (and mudrocks in general) requires a set of integrated tools. This is because mudrocks are heterogeneous at vastly different scales. Linking the large-scale heterogeneity (e.g., sedimentary structure, and rock types) to the small-scale variations (e.g., micrite textures, pore types, and organic content) is essential for hydrocarbon exploration. A number of tools will be examined using the case study of the Tuwaiq Mountain and the Hanifa formations, Saudi Arabia as a prelude to work to be done on the Shublik Formation, Alaska. The work presented here is part of a Masters thesis done in Colorado School of Mines (Al Ibrahim, 2014). At this location, five lithofacies have been identified from core and thin sections (Figure 1). The Tuwaiq Mountain Formation is composed of shelf-derived wackestones to grainstones, and is dominated by a highstand systems tract. The Hanifa Formation is composed mainly of laminated mudstones and wackestones, capped by a sequence boundary and a lowstand systems tract composed of packstones and anhydrite.

The sequence stratigraphic framework was constructed by integrating geologic observations with mathematical and statistical analysis (Figure 2). Multi-scale automated electrofacies analysis using self-organizing maps and hierarchical clustering shows good correlation with observed lithological variations and interpreted sequence stratigraphy. Elemental analysis allows for the creation of redox and paleoproductivity indices. High total organic carbon content up to 14% TOC occurs in transgressive system tracts and correlates well with intervals with suboxic to anoxic conditions and relatively high paleoproductivity. Cyclostratigraphic analysis done with borehole images using the Modified Fischer Plot (MFP) approach shows distinct thinning and thickening stacking patterns. These are correlative with independently defined sequence stratigraphic surfaces. Highstand and lowstand system tracts show thickening pattern in the MFP, i.e. moving to the right, while the highstand system tract show a thinning pattern, i.e. moving to the left. Finally, spectral analysis of intervals thickness shows viable correlation with Milankovitch cycles.

High-resolution scanning electron and confocal microscope images show different micrite textures ranging from porous subrounded to tightly fused micrite (Figure 3). Variations in texture are mainly attributed to sediment composition. Shelf-derived sediments are dominant in the highstand systems tract and are metastable, resulting in recrystallization and tight micrite formation. Transgressive systems tracts contain a relatively higher proportion of coccoliths. These are relatively more stable, so a porous texture is observed due to lack of recrystallization. Coccoliths can also bind with organic

matter, which results in an increase in settling velocity, leading to enhanced preservation of organic matter.

References

Al Ibrahim, M. A., 2014, Multi-scale sequence stratigraphy, cyclostratigraphy, and depositional environment of carbonate mudrocks in the Tuwaiq Mountain and Hanifa formations, Saudi Arabia: Colorado School of Mines, MSc Thesis, 194 p.

Acknowledgments

Data and funding for this research are generously provided by Saudi Aramco. Schlumberger provided generous access to their confocal microscope for this work.

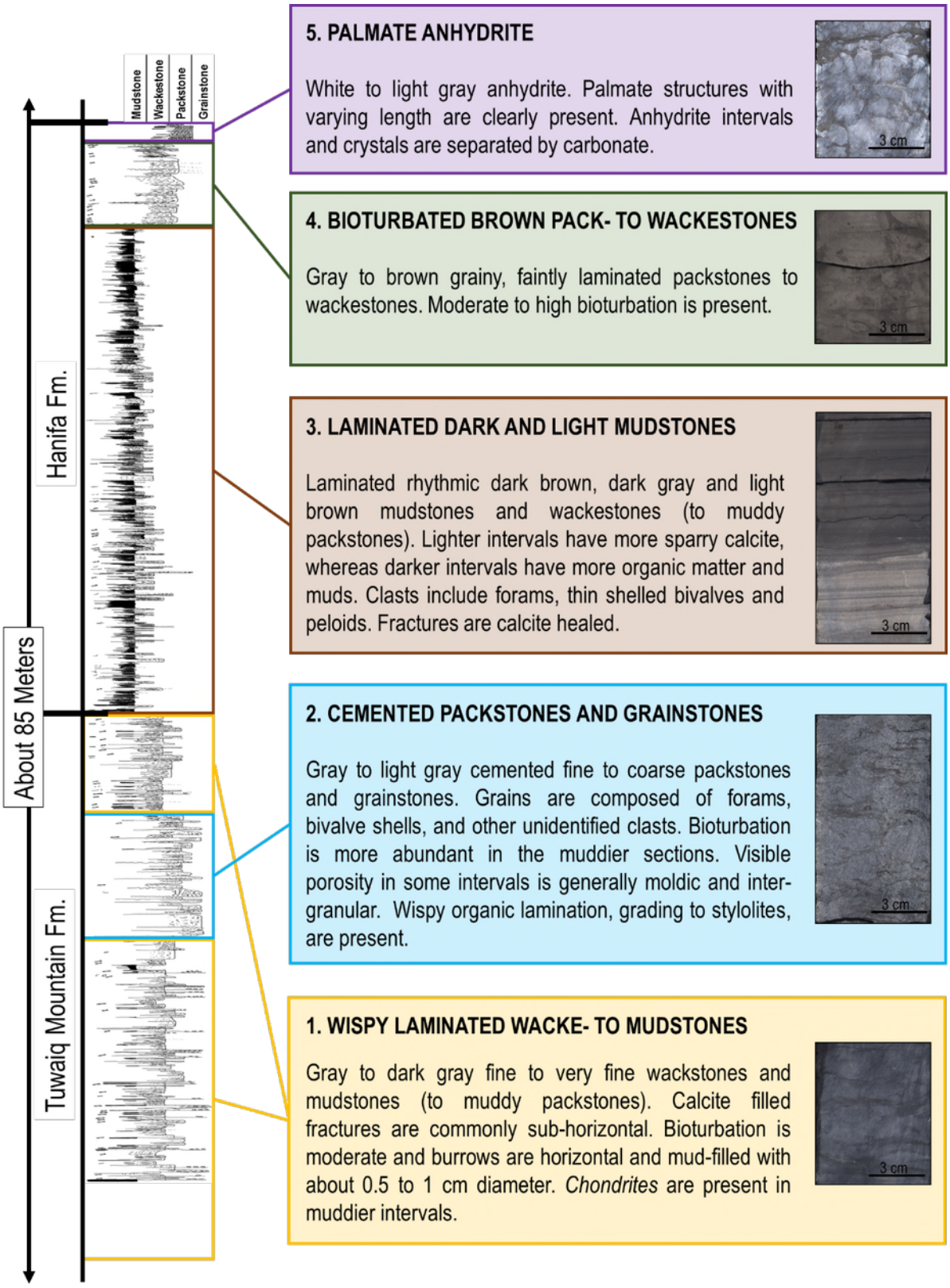

Figure 1. A general summary of the lithofacies identified in the studied interval of the Tuwaiq Mountain and Hanifa formations basinal deposits.

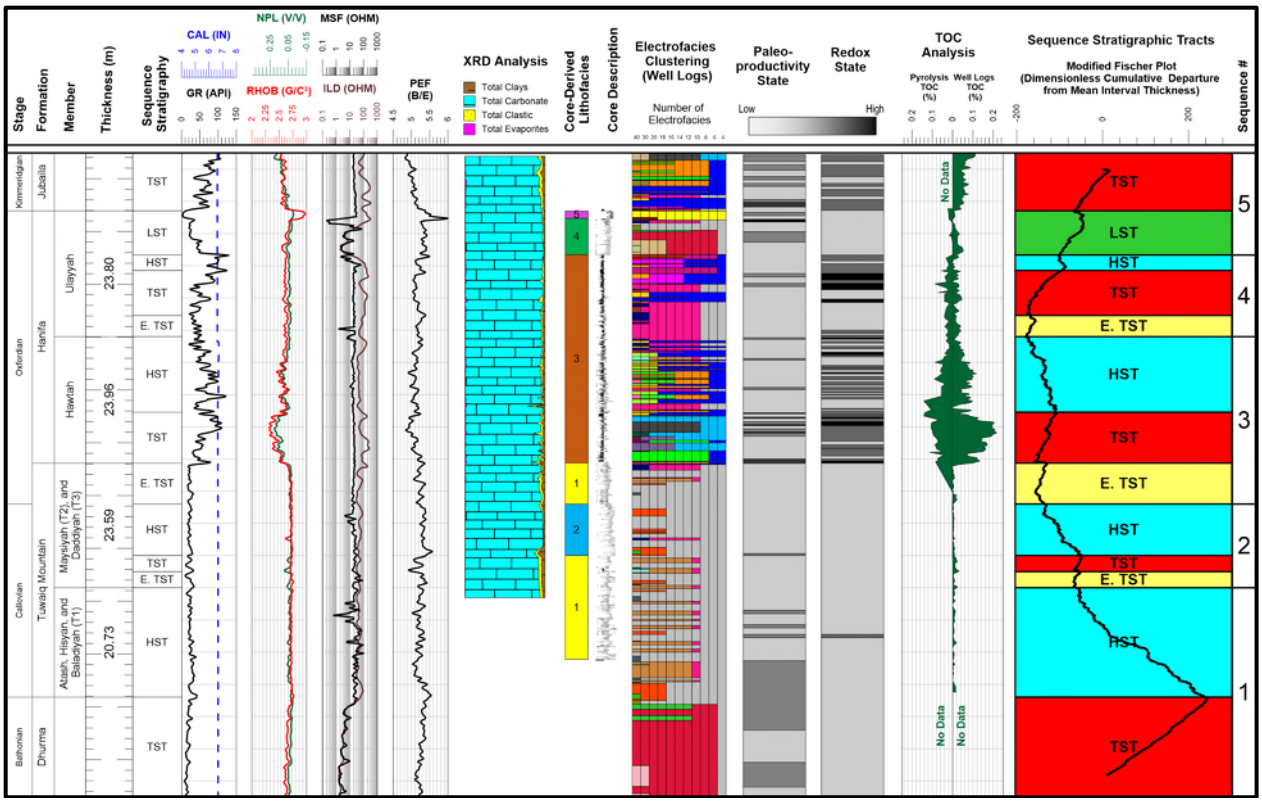

Figure 2. Summary of analysis done of the Tuwaiq Mountain and Hanifa formations. The interval is predominantly composed of carbonates (XRD). Five lithofacies have been identified in the core. These correspond well with electrofacies analysis using well logs. Paleoproductivity and redox state correlate with TOC values estimated from well logs and measured from pyrolysis. Cyclostratigraphic analysis is done using the Modified Fischer Plot method. It shows good correlation with the sequence stratigraphic framework developed. The sequence stratigraphic framework is shown where tst is transgressive systems tract, E. TST is early transgressive systems tract, HST is highstand systems tract, and LST is lowstand systems tract.

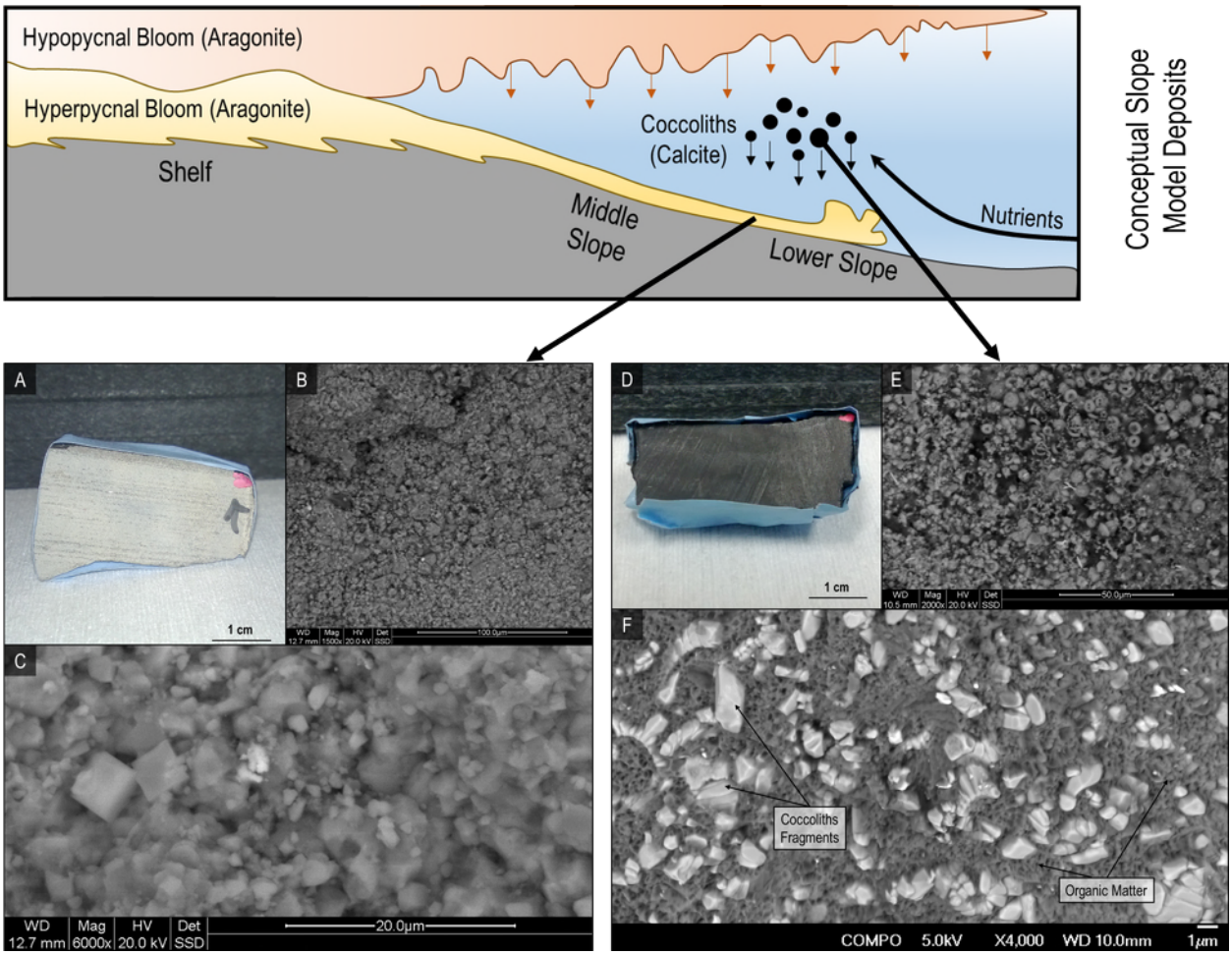

Figure 3. Two micrite textures were identified in the Hanifa formations basinal deposits. Lighter-colored rocks are mainly composed of euhedral micrite. Darker-colored rocks are mainly composed of coccoliths fragments and organic matter.

BASIN AND PETROLEUM SYSTEM MODELING IN THE LOS ANGELES BASIN, CALIFORNIA

Lauren E. Schultz, Allegra Hosford Scheirer, Ken Peters[1], Steve Graham
Department of Geological and Environmental Sciences, Stanford University
[1]*Also at Schlumberger Information Solutions*

This project examines the Los Angeles Basin of California through 1D and 2D basin and petroleum system modeling processes. The geologic context of the basin provides several challenges from a basin modeling perspective, especially regarding the complex tectonic history of the basin. The Los Angeles basin formed as a pull-apart basin, resulting from the transverse motion along several local NW trending fault zones, and producing significant clockwise block rotation (Biddle, 1991). The basin is subdivided into several blocks by faults that cross-cut the basin, including the Newport-Inglewood deformation zone, which cuts through the eastern part of basin, separating southwestern and central blocks, and the Whittier fault zone, which cuts through the basin to the west, separating the central and northwestern blocks (Wright, 1991). The basin is additionally cross-cut by a series of east-trending faults, which form the boundary between the Transverse Ranges and Peninsular Ranges to the North. Structurally, the basin sits on a deep NW trending basement trough as deep as 31,000 ft and the overlying sedimentary strata are significantly deformed by faulting and folding, which serve as the predominant source of trapping for the petroleum generated in the basin (Yerkes et al., 1965).

The Los Angeles Basin presents an especially valuable opportunity for basin and petroleum system modeling due to its impressively high hydrocarbon productivity relative to sediment volume (Yerkes et al., 1965), source rock TOC as high as 10-16% (Jeffrey et al., 1991), and the geochemical diversity of the produced oils (Peters et al., 2014). In this work, we present a preliminary 1D model of the American Petrofina Corehole #1 well located in the middle of the depocenter where the presumed Mohnian-aged source rock is thermally mature. With a total depth of more than 21,000 feet, the well only penetrates into upper Repettian strata; deeper units are presumed on the basis of seismic and gravity data, including a basement depth at nearly 30,000 feet. The Pliocene Pico and Repetto formations are reservoir rocks that overlie the Mohnian source rock. Custom black oil kinetics are used; these derive from a Mohnian Lower Modelo Formation (Monterey-equivalent) sample taken from Bellagio Road north of Sunset Blvd. Calibration data comprise observed subsurface temperatures and vitrinite reflectance. Future 2D models will transect the basin to provide a perspective on the influence of the geometry and structure of the basin, as well as petroleum migration and trapping mechanisms.

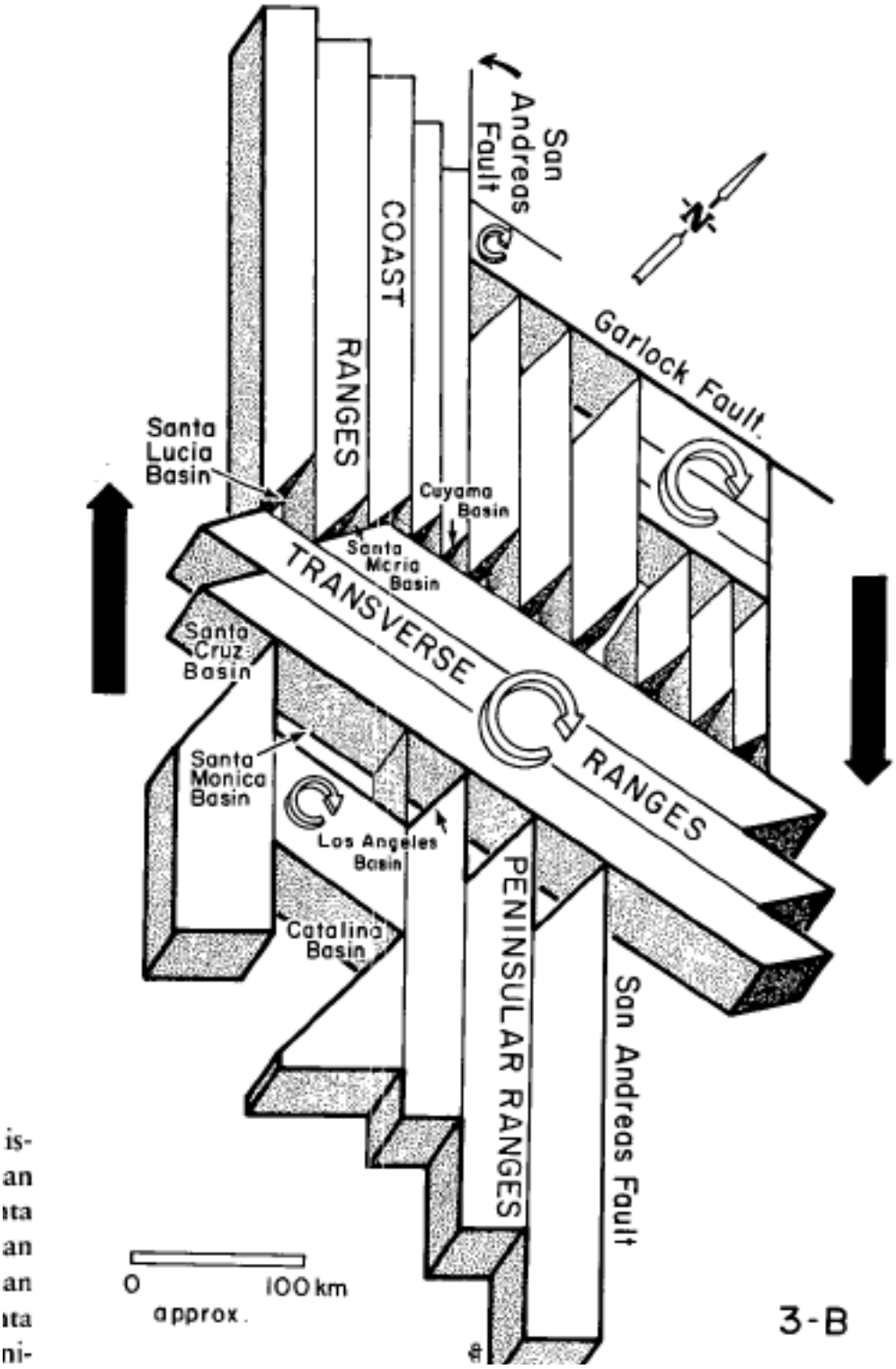

Figure 1. Tectonic context of the Los Angeles Basin, situated near the intersection of the Peninsular and Transverse Ranges, as well as the Coast Ranges to the West. From Luyendyk et al., 1980.

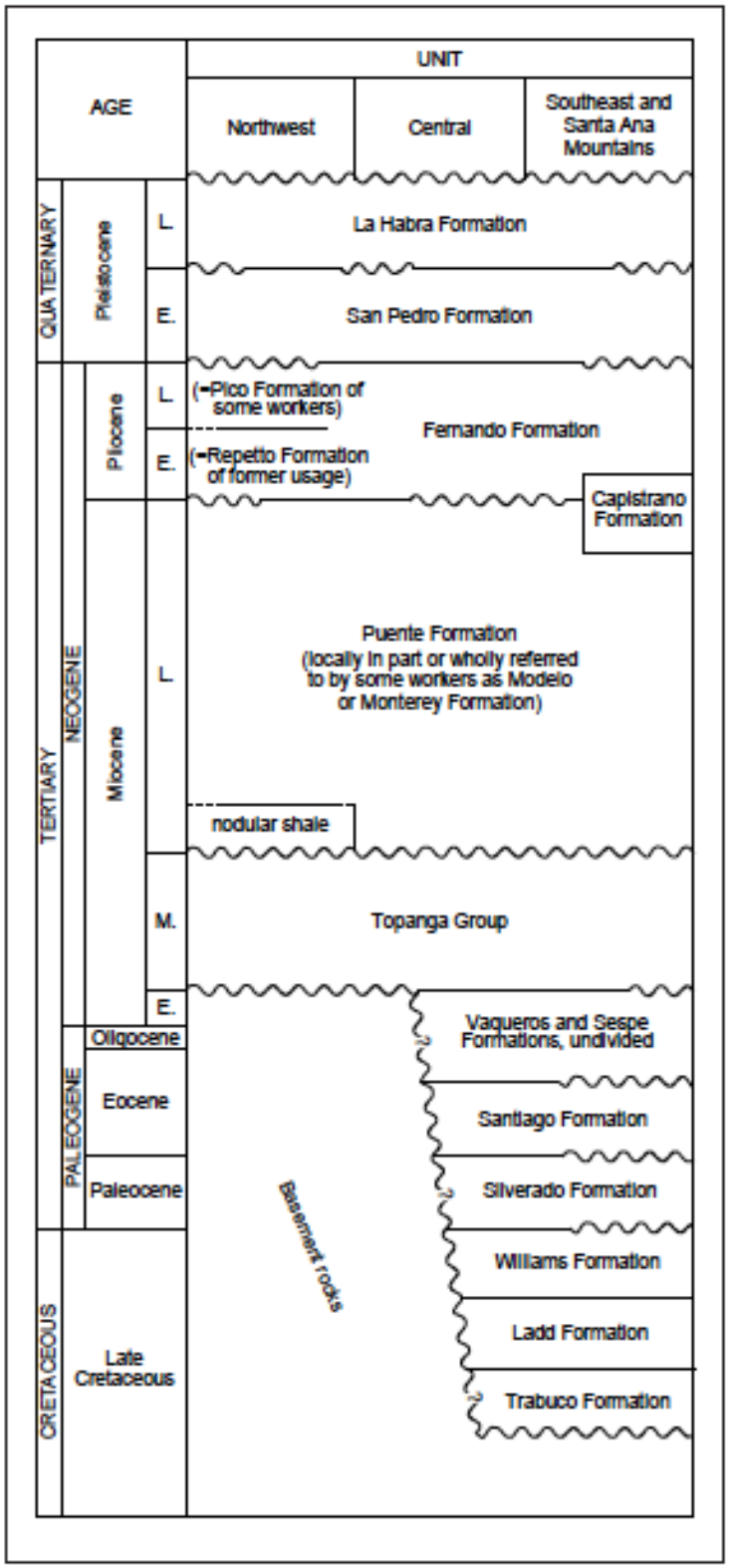

Figure 2. Stratigraphy of the Los Angeles basin with source rocks, including the nodular shale and Puente/Monterey Fm and important reservoirs, including the Pico and Repetto. From Beyer, 1995.

References

Biddle, K. T. "The Los Angeles basin: an overview." Active margin basins: AAPG Memoir 52 (1991): 5-24.

Jeffrey, Alan WA, Hossein M. Alimi, and Peter D. Jenden. "Geochemistry of Los Angeles Basin oil and gas systems." Active margin basins: AAPG Memoir 52 (1991): 197-219.

Peters, K.E., Ramos, L.S., Zumberge, J.E., Wright, T.L. "Petroleum Systems in the World's Richest Petroliferous Basin, Los Angeles, California." Search and Discovery Article #80386 (2014).

Wright, Thomas L. "Structural geology and tectonic evolution of the Los Angeles Basin, California." Active Margin Basins 52 (1991): 35-134.

Yerkes, Robert F., et al. "Geology of the Los Angeles basin, California: an introduction." US, Geol. Surv. Prof. Pap. 420 (1965).

INTEGRATING BASIN MODELING WITH SEISMIC ATTRIBUTES THROUGH ROCK PHYSICS

Wisam AlKawai, Tapan Mukerji[1], Steve Graham
Department of Geological and Environmental Sciences, Stanford University
[1]Department of Energy Resources Engineering, Stanford University

Introduction

In this study, we explore the impact of different rock physics models on the link between basin modeling outputs and their associated seismic attributes. Basin and Petroleum System Modeling (BPSM) is critical in hydrocarbon exploration because of its ability to assess generation, migration, and accumulation of petroleum in a sedimentary basin based on the simulated thermal history resulting from sedimentary deposition and erosion (Peters, 2009). BPSM is a dynamic numerical modeling scheme that involves solving coupled partial differential equations with moving boundaries. Outputs from the computation include vitrinite reflectance, temperature, effective stress, and porosity. Traditionally, these outputs are compared with existing data to calibrate basin models. However, most types of calibration data such as vitrinite reflectance are limited to the borehole vicinity. Certain basin modeling outputs such as porosity, effective stress, pore pressure, and pore fluids saturation—when combined appropriately with rock physics models—can result in estimations of seismic attributes. These estimates allow a basin model to be calibrated on the regional scale.

In seismic exploration, low frequency seismic data (<10 Hz) are particularly important because they are less attenuated than high frequency data and penetrate to deeper targets (Dragoset and Gabitzsch, 2007). Impedance inversion from band-limited seismic data requires as input information about the low frequency background trend. This is generally accomplished by combining seismic data with background models built from well-log data and depth trends because typical seismic data lack low frequencies (Cerney and Bartel, 2007). One challenge in the seismic inversion process is building a robust background model when well-log data are sparse or absent. Combining basin modeling outputs with appropriate rock physics models can help to constrain the background model for seismic impedance inversion.

The data set used in this study is the E-Dragon II data in the Gulf of Mexico that include seismic data and well-log data. First, we use well-log data to define relations between seismic velocities and porosity, effective stress, and pore pressure using well-known rock physics modes. Then, we obtain basin modeling estimates of seismic velocities using different rock physics models and compare these estimates with well-log velocity data for calibration. After that, near angle partial stack seismic data are inverted into elastic impedance to show an example of an attribute that can be used to calibrate a basin model. We further test the concept of using basin modeling estimates of seismic velocities and densities to condition these background models.

Method

The first part of the study is rock physics modeling. The goal of this part is to build models that describe changes of seismic velocities Vp and Vs as a function of porosity, pore pressure, and effective stress. Vp-Vs relationship was established using Castagna's (1993) model that fit the measured Vp and Vs sonic log data for the well ST-168. Shear wave sonic logs in the other wells were not measured but estimated from this Vp-Vs relationship. After that, we defined lihofacies at SS-187 based on the volume of shale (Vshale) calculated from the gamma ray log. We modeled the Vp-porosity relation for the different lithofacies by choosing from well-known rock physics models such as the constant cement model (Avseth et al., 2000), the friable sand model (Dvorkin and Nur, 1996), and Han's empirical relation (1986), as appropriate for each lithofacies. Finally, we defined normal compaction trends of Vp for both sandstone and shale at the well SS-187 using published compaction trends in the Gulf of Mexico by Dutta et al. (2009) to characterize changes in Vp with effective stress.

The second part is 1D basin modeling at wells SS-187 and SS-160 to understand the impact of applying different rock physics models on calibrating the basin models using Vp and Vs. We used a commercial software package, PetroMod, for the basin modeling. At the start, the simulated 1D basin models were initially calibrated to mud weights and porosity data by adjusting the porosity and permeability compaction curves of the lithofacies. Basin modeling outputs were related to seismic velocities using three different approaches. The first estimates of Vp and Vs are the default outputs that were calculated based on the concept of Terzaghi's compressibility (Terzaghi, 1943) from the porosity compaction curve with depth (Hanstschel and Kauerauf, 2009). The second approach combined the basin modeling porosity output with the calibrated Vp-porosity rock physics models to get Vp and then obtained Vs using the established Vp-Vs relationship. The last estimate of Vp was based on Eaton's model (1975) of the Vp-effective stress relationship. The normal compaction trend in each age interval in the model was calculated by a volumetrically weighted arithmetic average of the sandstone and shale Vp compaction trends. Then, Vs was calculated again from the Vp-Vs relationship.

The last part is seismic inversion of the near angle stack data into near angle elastic impedance. The goal of this part is to show an example of a seismic attribute that can be used as calibration for a basin model and demonstrate how basin modeling outputs can constrain the background model, which is critical in the inversion process. The background model for the inversion was based on Connolly's (1999) equation for elastic impedance. In the inversion process, we built the background model from P and S wave sonic logs as well as the density logs at the wells SS-160 and ST-143. Then, we tested the change in the inversion results with different weights assigned to the background model. Following that, we took the basin modeling estimates of Vp and Vs associated with different rock physics models in the second part of the study and combined them with the basin modeling density output to build background models.

Rock Physics Modeling

Figure 1 shows the results from modeling Vp-porosity relationships. Below 8000 ft, the Vp-porosity relationship was modeled with Han's empirical relation (1986) for lithofacies with Vshale less than 0.5 and with the friable-sand model (Dvorkin and Nur, 1996) for higher Vshale. Above 8000 ft, the relationships were modeled with the constant-cement model (Avseth et al., 2000) for all lithofacies. These results of Vp-porosity modeling

suggest that below 8000 ft, the Vp-porosity trends generally become steeper showing more significant increase in velocity with decrease in porosity. Figure 2 shows the Vp normal compaction trends for sandstone and shale. The trend for shale in figure 2-a overestimates Vp below 12000 ft and this can be related to the high pore pressure observed below that depth in the mud weight data.

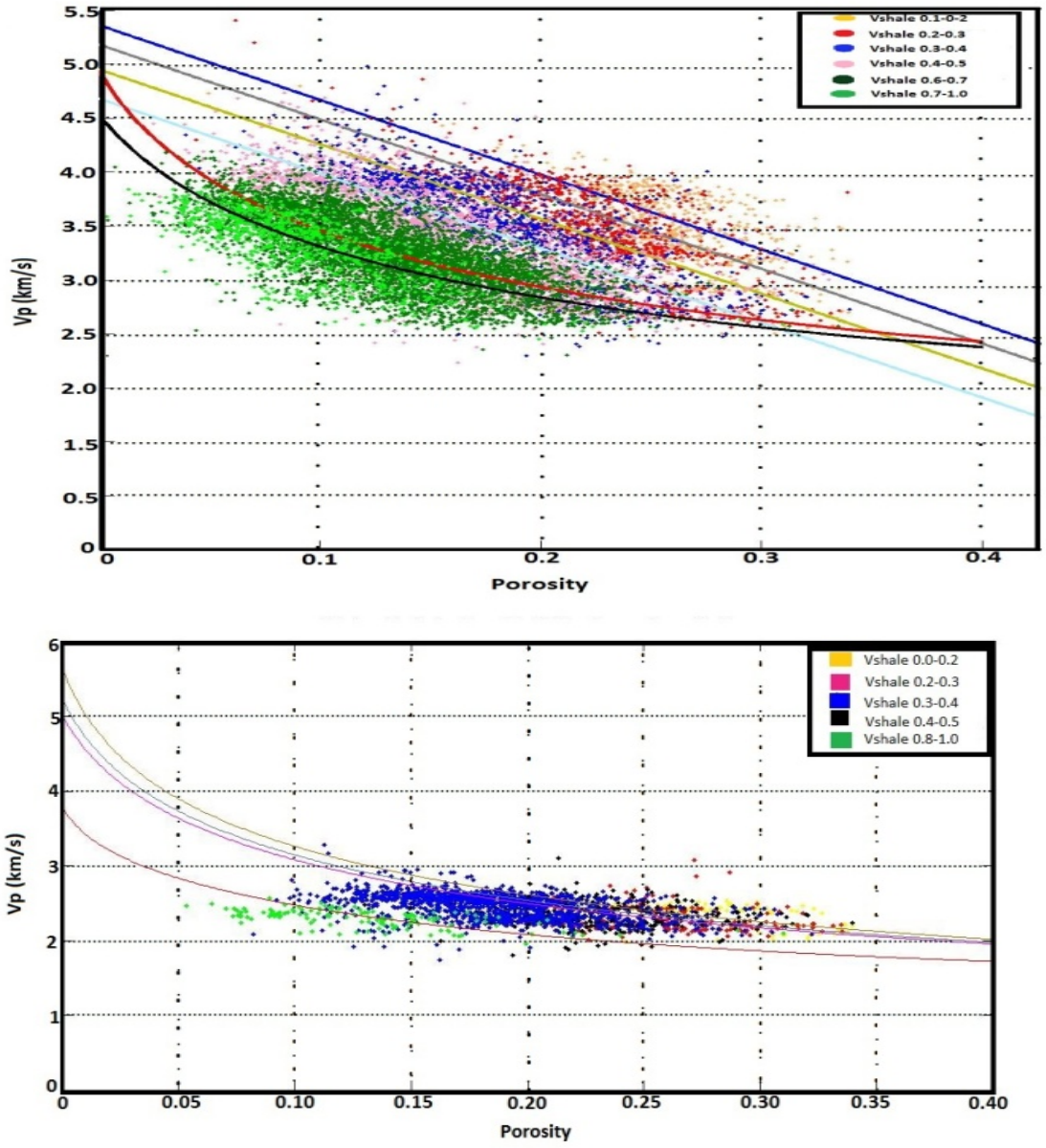

Figure 1. Vp-porosity models below 8000 ft (top) and above 8000 ft (bottom).

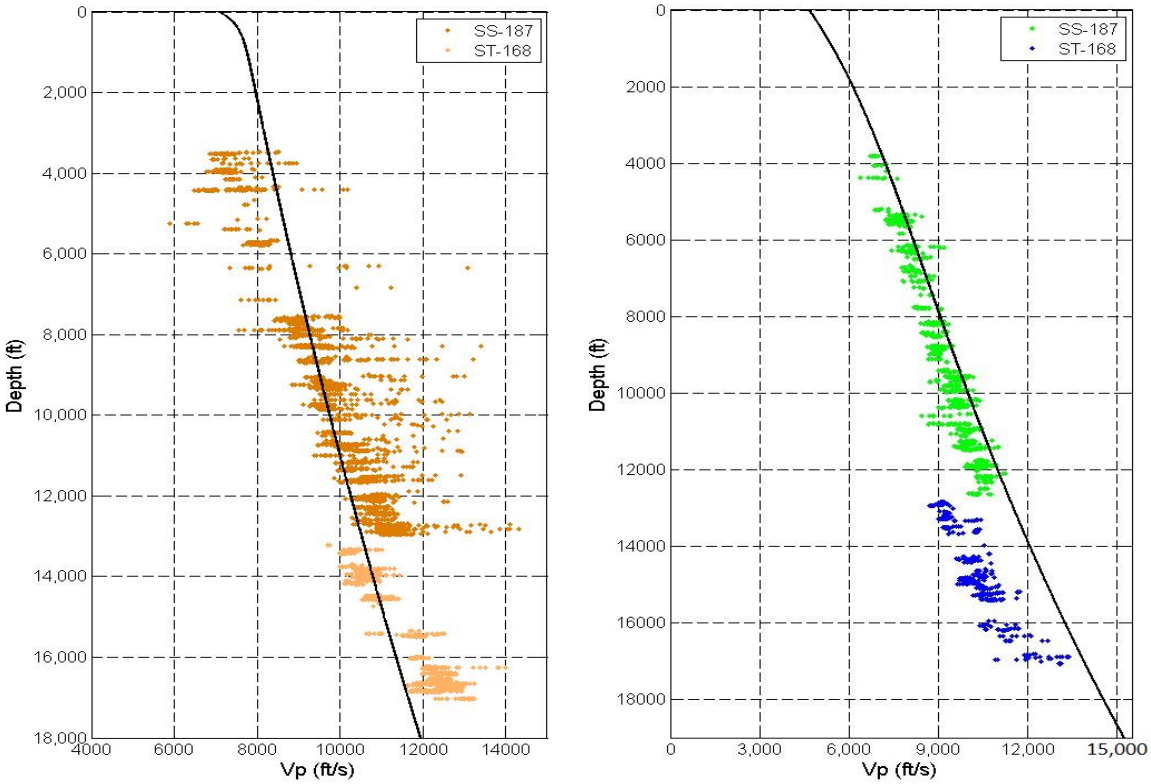

Figure 2. Vp normal compaction trend for sandstone (left) and shale (right)

Basin Modeling Vp Calibration

Figure 3 is a comparison of 1D basin modeling Vp estimates at SS-187 and how well each estimate matches calibration data. The calibration data were obtained from the measured P-wave sonic log by considering the average sonic Vp values. The first Vp output was directly calculated without using the rock physics model and this estimate seems to overestimate the observed Vp values. The second Vp estimate was obtained by transforming basin modeling porosity output into Vp using the previously established Vp-porosity models and this model seems to match the calibration data very well. The third Vp estimate was calculated by transforming the basin modeling outputs of effective stress, lithostatic stress, and hydrostatic stress into Vp along with the normal compaction values of Vp using Eaton's (1975) method. This Vp output matches the calibration data but its velocity structure is less detailed than the second output.

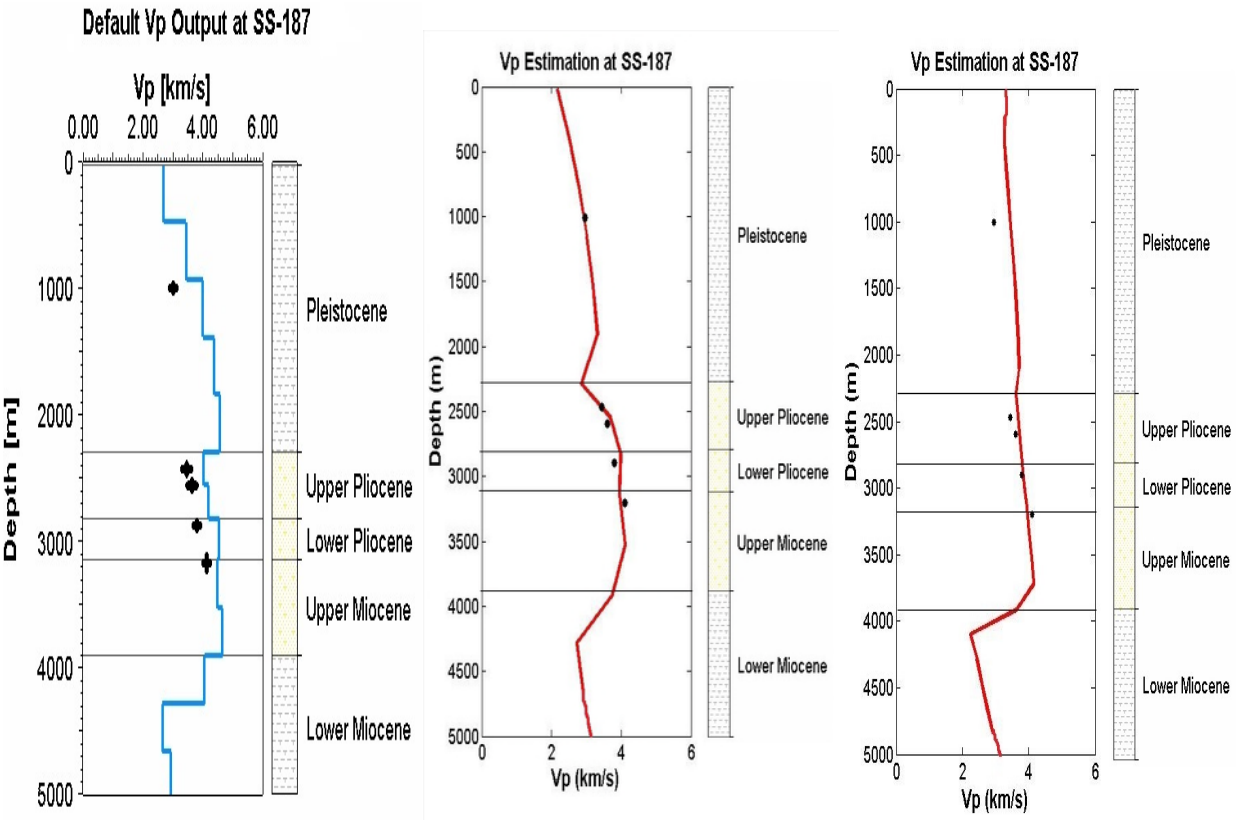

Figure 3. Basin modeling Vp estimates without rock physics models (left), from Vp-porosity models combined with porosity output (middle), and from Vp-effective stress model combined with stress outputs (right). The dots indicate the calibration data.

Elastic Impedance Background Models

Figure 4 shows near angle elastic impedance background models that were constrained with different Vp, Vs, and density data. The first model was built from the well-log data as discussed previously. The second model was built from pseudo well logs generated from the basin modeling density output as well as estimates of Vp and Vs based on Vp-porosity models. The third model was similar to the second one except that Vp and Vs are the ones derived from the Vp-effective stress relationship. The second model better matches the model built from the measured well-log data and is much more detailed than the third model.

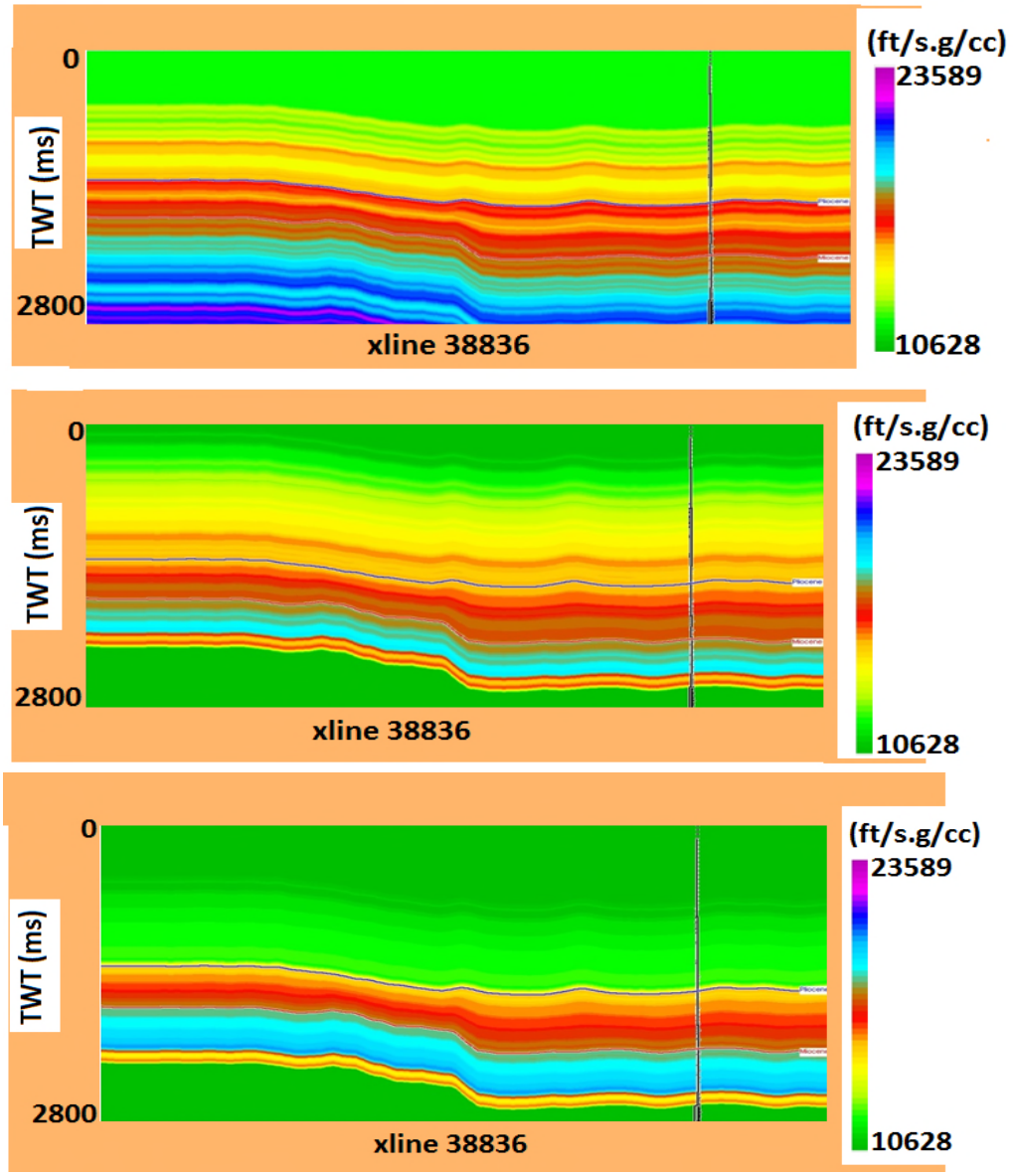

Figure 4. Elastic impedance background models based on measured well-log data (top), basin model density output and estimated Vp and Vs from Vp-porosity models (middle) and basin model density output and estimated Vp and Vs from Vp-effective stress model (bottom).

Conclusions

In this research, we have learned that rock physics is the key when linking basin modeling with seismic technology. The link between basin modeling and seismic attributes is a two-way link such that seismic attributes can provide calibration data for basin models that are extensive over a large spatial area and basin modeling can constrain the process of building background models and low frequency trends used for imaging and impedance inversion. Refining the link between basin modeling outputs and seismic attributes depend on the rock physics models applied. We observed in this study that estimating Vp by combining basin modeling porosity output with Vp-porosity models results in a more

detailed velocity structure because we are accounting for more effects that change Vp. Therefore, it is an important practice to first establish rock physics models that describe changes in seismic attributes with rock properties and then apply them to link basin modeling with seismic attributes.

Acknowledgements:

The authors acknowledge "well-log data Copyright (2013) IHS Energy Log Services Inc." We thank Schlumberger/WesternGeco for providing the seismic data. We also thank David Greeley from BP for his great support. Funding and participation in this research is made possible through the support of the Stanford Basin and Petroleum System Modeling, Stanford Center for Reservoir Forecasting, and Stanford Rock Physics industrial affiliate research programs and through Saudi Aramco Scholarship.

References:

Avseth, P., Dvorkin, J., Mavko, G., & Rykkje, J., 2000, Rock physics diagnostics of North Sea sands: Link between microstructure and seismic properties, Geophys. Res. Lett., 27, 2761–2764.

Castagna, J. P., Batzle, M. L., and Kan, T. K., 1993, Rock physics--The link between rock properties and AVO response in John P. Castagna and Milo M. Backus, Eds., Offset-dependent reflectivity -- theory and practice of AVO analysis: Investigations in Geophysics Series, Soc. Expl. Geophys., 8, 135-171.

Cerney, B., and Bartel, D. C., 2007, Uncertainties in low-frequency acoustic impedance models, The Leading Edge, 26, 1, 74-87.

Connolly, P., 1999, Elastic impedance: The Leading Edge, 18, 438–452.

Dragoset, B., and J. Gabitzsch, 2007, Introduction to this special section: Low frequency seismic, The Leading Edge, 26, 1,34-35.

Dutta, T., Mavko, G., Mukerji, T. and Lane, T. 2009, Compaction trends for shale and clean sandstone in shallow sediments, Gulf of Mexico: The Leading Edge, 28, No.5, 590-596.

Dvorkin, J., and A. Nur, 1996, Elasticity of high-porosity sandstones: Theory for two North Sea datasets, Geophysics, 61, 1363-1370.

Eaton, B. A., 1975, The equation for geopressure prediction from well logs: SPE 5544.

Han, D., 1986, Effects of porosity and clay content on acoustic properties of sandstones and unconsolidated sediments: Ph.D. dissertation, Stanford University.

Hantschel, T., Kauerauf, A., 2009. Fundamentals of Basin Modeling, Springer-Verlag, Heidelberg, 425 pp.

Peters, K. E., 2009, Getting Started in Basin and Petroleum System Modeling. American Association of Petroleum Geologists, AAPG CD-ROM #16.

Terzaghi, K., 1943, Theoretical soil mechanics: John Wiley & Sons, Inc., New York, 510 pp.

INVESTIGATING THE IMPACT OF ALLOCHTHONOUS SALT AND OVERPRESSURE ON PETROLEUM SYSTEM DEVELOPMENT IN THE THUNDER HORSE MINIBASIN BY INTEGRATING 3D BASIN AND PETROLEUM SYSTEM MODELING WITH QUANTITATIVE SEISMIC INTERPRETATION

Wisam AlKawai
Department of Geological and Environmental Sciences, Stanford University

Continuing successful exploration in the northern U.S. Gulf of Mexico basin requires a thorough understanding of the evolution of the essential elements of the petroleum system. The basin is a small ocean basin in which salt tectonics associated with the interaction between the Jurassic Louann Salt and the loaded sediments defined the structural framework of the basin (Galloway, 2005). Allochthonous salt bodies play a major role in the development of the petroleum system as they retard the thermal maturity of source rocks below them due to their high thermal conductivity (McBride et al., 1998; Stover et al., 2001). Interaction between sedimentation and allochthonous salt induced overpressure development and dissipation following the post rift phase to the present day. Overpressure of the sediments, if specifically caused by disequilibrium compaction, tends to enhance the porosity of the sediments and lower the thermal conductivity, which reduces thermal diffusion in strata underlying overpressured zones that can enhance thermal maturity of source rocks (Jones, 1969; Mello and Karner, 1996). In fact, detecting overpressure and understanding its development is critical for deepwater drilling in the northern U.S. Gulf of Mexico basin to plan safe drilling.

The Thunder Horse minibasin in figure1 of southern Mississippi Canyon is one of the most productive minibasins in the northern deep Gulf of Mexico. The production is from the Miocene reservoirs trapped in the turtle structure in figure 2. The Thunder Horse area is a good region to examine the impact of allochthonous salt evolution along with the overpressure development on the petroleum system in. Previous work by Matt el al. (2004) showed that the maturation of the Turonian source is delayed in the Thunder Horse minibasin relative to its maturation in the Mensa minibasin due to the evolution of the Thunder Horse salt body that overlies the Turonian source rock. This goal of this study is to utilize basin and petroleum system modeling to investigate the impact of allochthonous salt evolution and overpressure development on petroleum system development.

The following sections describe the proposed parts of the study and the challenges to be addressed in each.

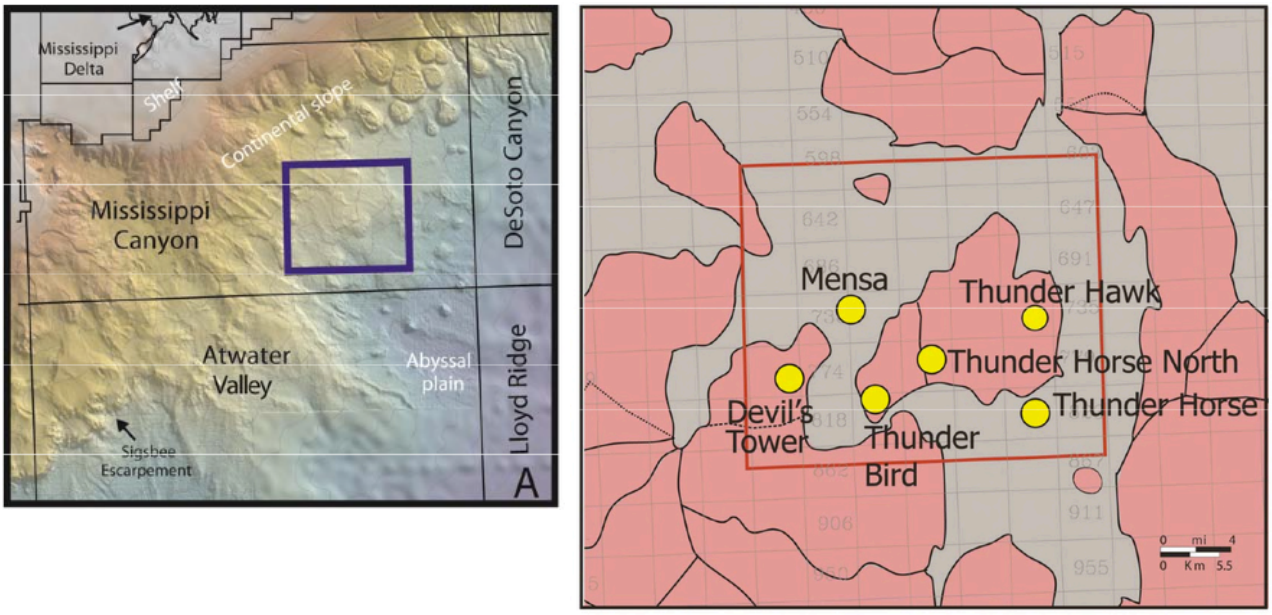

Figure 1. Location of Thunder Horse field from Cepeda et al (2010).

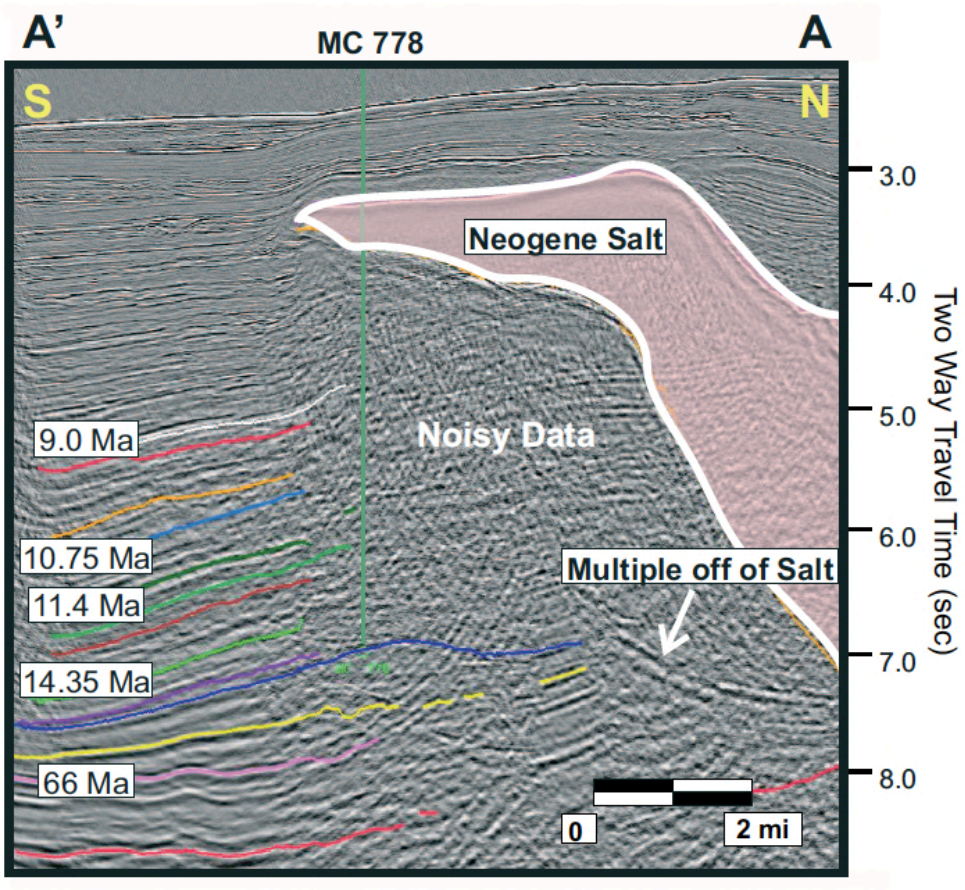

Figure 2. Seismic line across the subsalt turtle structure in the Thunder Horse area from Lapinski et al. (2004).

Quantitative Seismic Interpretation

Application of quantitative seismic interpretation (QSI) techniques in previous studies to interpret lithofacies and saturating pore fluids showed good results at the reservoir scale (Mukerji et al., 2001; Avseth et al., 2007). Quantitative seismic interpretation starts with interpreting well-log data combined with statistical rock physics to build representative probability distribution functions (pdfs) of the different lithofacies that are likely to exist at the reservoir scale. Then, the pdfs are used to classify the most likely lithofacies at each point based on the control of seismic attributes (i.e. acoustic and elastic impedances). An important advantage of this approach is interpreting the lithofacies over the spatial extent of the seismic attributes, not just at discrete well locations. The regional interpretation of lithofacies is especially important when dealing with heterogeneous deposits such as turbidites. Extending (QSI) techniques at the basin scale can provide important control for basin and petroleum system modeling lithofacies input. Also, it can provide a more careful constraint on the rock physics models describing the elastic properties of the lithofacies, which can be crucial when using basin and petroleum system modeling to investigate overpressure development. Of course, extending QSI techniques at the basin scale requires new techniques of defining representative lithofacies that carefully consider non-stationarity. Also, QSI typically results in probability maps of the lithofacies and basin and petroleum system modeling typically handles a single input of lithofacies within a defined interval in the model. So, it is important to define the right practices that best utilize the information from the lithofacies probability maps resulting from QSI.

Overpressure Investigation

The development of overpressure in the sediments in the northern Gulf of Mexico basin necessitates developing good techniques to predict pore pressure for safe drilling (Giles et al., 1999; Throndsen and Wangen, 1998; Yardley and Swarbrick, 2000; Yardley et al., 2004). Predicting pore pressure accurately requires understanding the mechanisms by which the overpressure developed through the geologic history of the basin. Disequilibrium compaction is believed to be the main mechanism of generating overpressure (Osborne and Swarbrick, 1997; Berhmann et al., 2006). Another mechanism that has been considered a possible source of overpressure is smectite to illite conversion. Plumley (1980), Berg and Harback (1982), and Bruce (1984) note the association of overpressure with the conversion of smectite to illite. Although some studies suggest that smectite-illite conversion is less important than disequilibrium compaction (Dutta, 1986 and 1988, Osborne and Swarbrick, 1997), other authors such as Audet (1995) argued that chemically releasing the bond water results in overpressure increase by as much as 30%. Shale compaction properties also change with the conversion of smectite to illite (Lahann et al., 2001, Lahann, 2002), which is reflected in density-effective stress data shown in figure 3. The exact mechanism by which the smectite to illite conversion causes overpressure is controversial. Bowers (2002) suggested inelastic unloading as the mechanism. Katahara (2006) proposed mechanical failure and he supported this proposed mechanism with density-slowness data in figure 4.

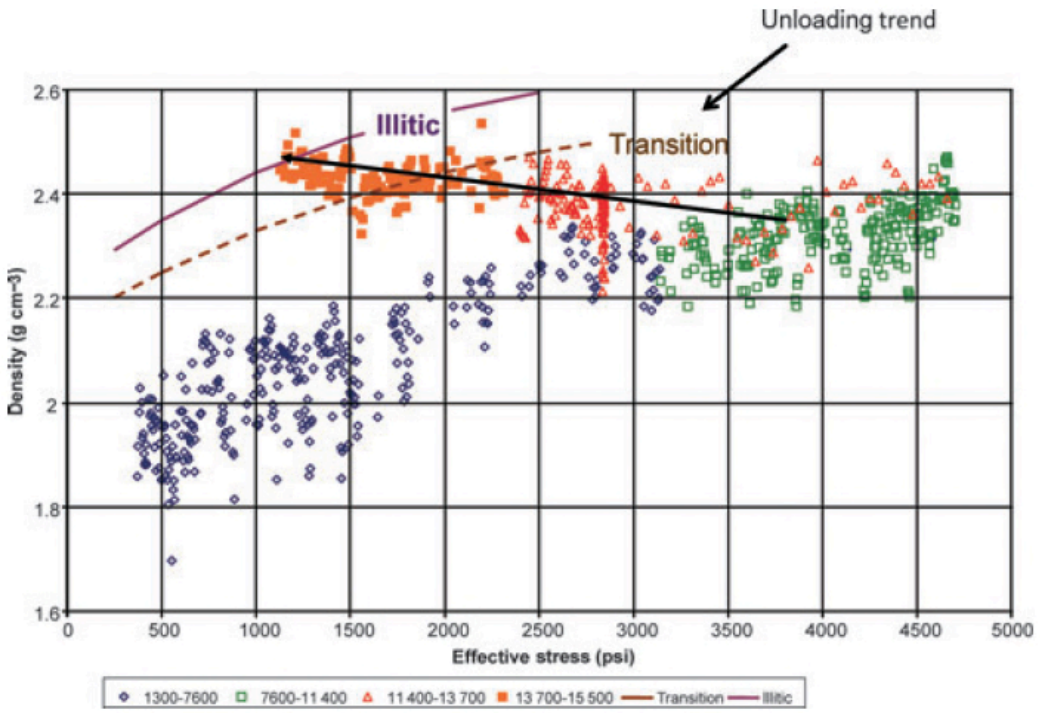

Figure 3. Change of density-effective stress relationship associated with smectite-illite conversion from Lahann et al. (2001).

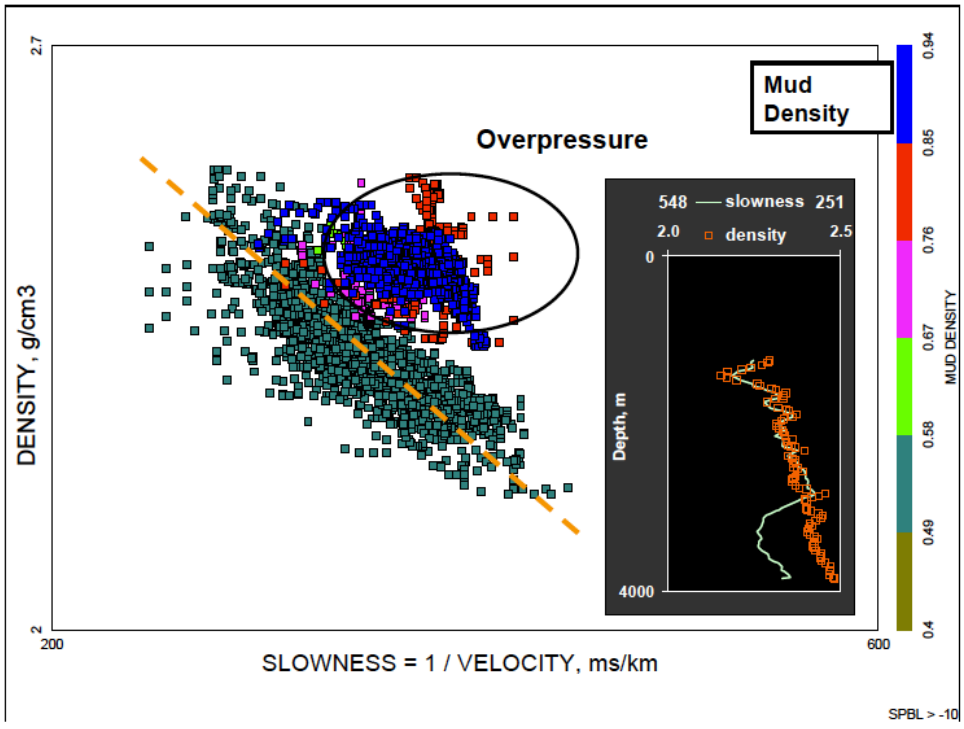

Figure 4. Density-slowness cross plot of overpressured sediments that are illite rich from Katahara (2006).

Characterizing the changes of pore pressure at least at the local scale requires careful characterization of the changes in shale compaction behavior associated with the smectite to illite conversion. A good way to characterize the changes of compaction behavior of shale is to combine to well-log data with available information about the clays from XRD and thin sections to build refined rock physics models. The rock physics models can then be used to choose the right transforms to interpret pore pressure from velocity and density information derived from pre-stack seismic inversion outputs. This step can allow more careful prediction of pore pressure using seismic attributes and it can also reveal some insights about the scale and detectability of the overpressure associated with the two potential mechanisms (i.e. disequilibrium compaction and smectite-illite conversion).

Another method that can be used to investigate the development of overpressure associated with these two potential mechanisms is basin and petroleum system modeling. Because the Gulf of Mexico is a salt basin, a basin model that carefully tries to address overpressure development requires a 3D structural restoration of the salt systems (Mello et al., 1995; Gibson, 2012). To try to investigate the smectite-illite conversion using basin modeling, the kinetics of the conversion of smectite to illite such as those by Pytte (1982) must be implemented. Then, the model should adjust the compaction of the shale where smectite transfers to illite. Combining this pore pressure prediction from basin modeling with pore pressure based on seismic attributes permits an assessment of the uncertainty and scale differences between these two methods. Also, combining them with information at the wellbore can provide some insights about the scale at which the two potential mechanism of overpressure operate in the basin.

Petroleum System Development

Having a 3D basin model that takes into account salt evolution and addresses overpressure development along with the causal mechanisms is a good tool to understand rigorously the impact of the allochthonous salt and the development of overpressure on the development of the petroleum system. Some authors investigated the impact of salt on the petroleum system, but these were limited to 2D (Diegel et al., 1995; McBride et al., 1998). Another 2D study by Stover et al. (2001) investigated the effect of both allochthonous salt evolution and overpressure development on the source rock maturation. We aim to use a 3D basin model that combines salt evolution with pore pressure estimation by using refined rock physics models that can potentially describe pore pressure changes associated with more than one potential mechanism. Understanding the impact of allochthonous salt evolution and overpressure development can be an important insight for success in future exploration.

References

Audet, D.M., 1995, Mathematical modeling of gravitational compaction and clay dehydration in thick sediment layers, Geophysical Journal International, 122, p. 283–98.

Avseth, P., T. Mukerji, and G. Mavko, 2007, Quantitative Seismic Interpretation. Applying Rock Physics Tools to Reduce Interpretation Risk, Cambridge Univ. Press, Cambridge, 359 pp.

Berg, R.R., Haback, M.F.,1982, Abnormal pressures in the lower Vicksburg, McAllen Ranch field, south Texas: Transactions of the Gulf Coast, Association of Geological Sciences, 32, p. 247–53.

Berhmann, J.H., Flemings, P.B., JOHN C.M., 2006, Rapid sedimentation, overpressure, and focused fluid flow, Gulf of Mexico continental margin. Scientific Drilling, 3, 12–17.
Bowers G.L., 2002, Detecting high overpressure, The Leading Edge, 21 (2), p. 174.

Bruce, C., 1984, Smectite dehydration – its relation to structure development and hydrocarbon accumulation in northern Gulf of Mexico Basin, AAPG Bulletin, 68, p. 673–83.

Cepeda, R., P. Weimer, and G. Dorn, 2010, 3D seismic stratigraphic interpretation of the Upper Miocene to Lower Pleistocene deepwater sediments of the Thunder Horse-Mensa area, Southern Mississippi Canyon, Northern Deep Gulf of Mexico: GCAGS Transactions, v. 60, p. 119-132.

Diegel, F. A., J. F. Karlo, D. C. Schuster, R. C. Shoup, and P. R. Tauvers, 1995, Cenozoic structural evolution and tectono-stratigraphic framework of the northern Gulf Coast continental margin, in M. P.A. Jackson, D. G. Roberts, and S. Snelson, eds., Salt tectonics: A global perspective: American Association of Petroleum Geologists Memoir 65, p. 109-151.

Dutta ,N.C., 1986, Shale compaction, burial diagenesis, and geopressures: a dynamic model, solution and some results, *in* Thermal Modeling in Sedimentary Basins, 1st IFP Exploration Research Conference (ed. Burrus J), p. 149–72, Technip, Paris.

Dutta, N.C., 1988, Fluid flow in low permeable porous media. Revue de L'Institute Francais du Petrol, 43, p. 165–80.

Galloway, W.E., 2005, Gulf of Mexico basin depositional record of Cenozoic North American drainage basin evolution: International Association of Sedimentologists Special Publication 35, p. 409-423.

Gibson, R., 2012, A methodology to incorporate dynamic salt evolution in three dimensional basin models: Application to regional modeling of the Gulf of Mexico, in K. E. Peters, D. J. Curry, and M. Kacewicz, eds., Basin Modeling: New Horizons in Research and Applications: AAPG Hedberg Series, no. 4, p. 103– 118.

Giles, M.R., Indrelid, S.L., Kuszir, N.J., Loopik, A., Meijerink, McNutt, J., Dijkstra, P., Heidug, W., Toth, J., Willis, M., Rutten, K., Elsinga, B., Huysse, P., Riviere, P., Burgisser, H., and Rowley, E., 1999, Charge and overpressure modelling in the North Sea: Multi-dimensional modelling and uncertainty analysis: in Fleet, A.J., and Boldy, S.A.R., eds., Petroleum geology

of Northwest Europe: Proceedings of the 5th Conference: London, Geological Society [London], p. 1313–1324.

Fleet, A.J., Boldy, S.A.R. (Eds.), Petroleum Geology of Northwest Europe: Proceeding of the 5th Conference, p. 1313–1324.

Jones, P. H., 1969, Hydrodynamics of geopressure in northern Gulf of Mexico basin, J. Pet. Technol. 21, p. 803-810.

Katahara, K. 2006, Overpressure and shale properties: stress unloading or smectite-illite transformation? 76th annual International Meeting, SEG, Expanded Abstracts, paper PPP 1.2, 1520–4.

Lahann, R.W., McCarty, D.K., Hsieh, J.C.C., 2001, Influence of clay diagenesis on shale velocities and fluid pressure, Offshore Technology Conference Proceedings, 33, p. 37–43.

Lahann, R.W., 2002, Impact of smectite diagenesis on compaction modeling and compaction equilibrium, *in* Pressure Regimes in Sedimentary Basins and Their Prediction (eds. Huffman, A.R., Bowers, G.L.) AAPG Memoir, 76, p. 61–72.

Lapinski, T., P. Weimer, and R. Bouroullec, 2004, Sequence stratigraphic evolution of Thunder Horse mini-basin, Mississippi Canyon, northern deep Gulf of Mexico: GCAGS Transactions, v. 54, p. 327-341.

Matt, V. Buroullec, R. Weimer, P. Roesink, J., 2004, Maturity History of the Source Rocks Below the Mensa and Thunder Horse Fields, Mississippi Canyon, Northeastern Gulf of Mexico, AAPG Annual Meeting Annual Meeting, Dallas, Texas, April 18-21, AAPG Search and Discovery Article #90026.

McBride, B., M. Rowan, P. Weimer, 1998, The evolution of allochthonous salt systems, northern Green Canyon and Ewing Bank (offshore Louisiana), northern Gulf of Mexico, AAPG Bulletin, v. 85, p. 1013-1036.

Mello, U. T., Karner, G. D., and Anderson, R. N., 1995, Role of salt in restraining the maturation of subsalt source rocks: Marine and Petroleum Geology, v. 12, p. 697-716.

Mello, U. T., and G. D. Karner, 1996, Development of sediment overpressure and its effect on thermal maturation: application to the Gulf of Mexico Basin: AAPG Bulletin, v. 80, p. 1367–1396.

Mukerji, T., Jorstd, A., Avseth, P., 2001. Mapping Lithofacies and Pore-Fluid Probabilities in a North Sea Reservoir: Seismic Inversions and Statistical Rock Physics, Geophysics, 66(4), p. 988-1001.

Osborne, M. J., and R. E. Swarbrick, 1997, Mechanisms for generating overpressure in sedimentary basins: a reevaluation: AAPG Bulletin, v. 81, no. 6, p. 1023–1041.

Plumley, W.J., 1980, Abnormally high fluid pressures: survey of basic principles, AAPG Bulletin, v. 64, no. 3, p. 414-422.

Pytte A., 1982, The kinetics of the smectite to illite reaction in contact metamorphic shales [M.A. Thesis]. Dartmouth College: Hanover, N.H. 78 pp.

Stover, S.C., P. Weimer, S. Ge, 2001, The effects of allochthonous salt evolution and overpressure development on source rock thermal maturation: a two-dimensional transient study in the northern Gulf of Mexico Basin, Petroleum Geosciences, 7, p. 281-290.

Throndsen, T., Wangen, M., 1998. A comparison between 1-D, 2-D and 3-D basin simulation of compaction, water flow and temperature evolution. In: Duppenbecker, S.J., Iliffe, J.E. (Eds.), Basin Modeling: Practice and Progress, vol. 141. Geologic Society, London, pp. 109–116. Special Publications.

Yardley, G.S., Swarbrick, R.E., 2000. Lateral transfer: a source of additional pressure? Marine and Petroleum Geology, 17, p. 523–537.

Yardley, G., Couples, G., Aplin, A., Yang, Y., Swarbrick, R.E., 2004. Lithology-based pore pressure prediction success: example from a Gulf of Mexico mini-basin, AAPG-SEPM Convention Proceedings A152, 2004.

KINETICS OF THE OPAL-A TO OPAL-CT PHASE TRANSITION IN LOW- AND HIGH-TOC SILICEOUS SHALE SOURCE ROCKS

Danica Dralus[1], Michael D. Lewan[2], Ken Peters[3]
Department of Geological and Environmental Sciences, Stanford University
[1]*Now at BP*
[2]*U.S. Geological Survey [now retired]*
[3]*Also at Schlumberger Information Solutions*

Marine diatoms deposit biogenic silica as amorphous opal-A. These deposits interact with saturating aqueous solutions, transforming to microcrystalline opal-CT and eventually quartz through a series of dissolution and precipitation reactions. The mineralogical changes cause corresponding changes in rock properties such as porosity, permeability, and acoustic response. The enhanced permeability and preserved porosity during these transitions may result in formation of diagenetic hydrocarbon traps. Successful exploitation of diagenetic traps in oil and gas exploration requires an understanding of how quickly these phase transitions occur and how natural variations in rock composition affect the transition rates.

The mechanisms underlying these phase transitions are still poorly understood (Stein and Kirkpatrick, 1976; Icenhower and Dove, 2000). Pore fluid chemistry partially controls the reaction rates, but it varies spatially and temporally due to variations in rock composition and flow rates. Earlier work employed hydrous pyrolysis experiments to determine the opal-CT to quartz phase transition kinetics for natural samples saturated with distilled water (Ernst and Calvert, 1969) and a buffered aqueous solution (Dralus, 2013). This study builds on that work by focusing on the kinetics of the opal-A to opal-CT phase transition, also determined through a series of hydrous pyrolysis experiments.

Two diatomite samples from the Miocene Monterey Formation, California, were used in the experiments, both from the same pedogenic weathering profile (Fig. 1). The samples each comprise approximately 80 wt% opal-A, 10 wt% phyllosilicates, and 6 wt% quartz. However, they have different amounts of TOC (0.36 wt% and 4.65 wt%) and contain a thermally mature Type II kerogen. The samples were mixed with a buffered aqueous solution that ensured the fluid maintained pH 7 or greater, and the mixtures were pyrolyzed at multiple temperatures between 280°C and 330°C. The pyrolysis experiments sampled the transition from opal-A to opal-CT and showed that the conversion in the high-TOC sample was significantly delayed compared to the low-TOC sample at the same temperature (Fig. 2). Data at multiple temperatures were combined to determine the activation energy and pre-exponential factor for the conversion of each of the two samples.

These kinetics data, combined with knowledge of the local thermal history, allow prediction of the opal-A to opal-CT transition depth in a basin. The estimated transition depth can then be used to predict diagenetic trap locations or identify mineralogical sources of crosscutting reflectors in seismic data. Low-TOC kinetics data provide a baseline for these estimates, whereas high-TOC kinetics data demonstrate the extent to which organic material affects the reaction rate in source rocks.

Fig. 1. Opal-A samples used in the pyrolysis experiments shown in the pedogenic weathering profile. The low-TOC sample is to the left.

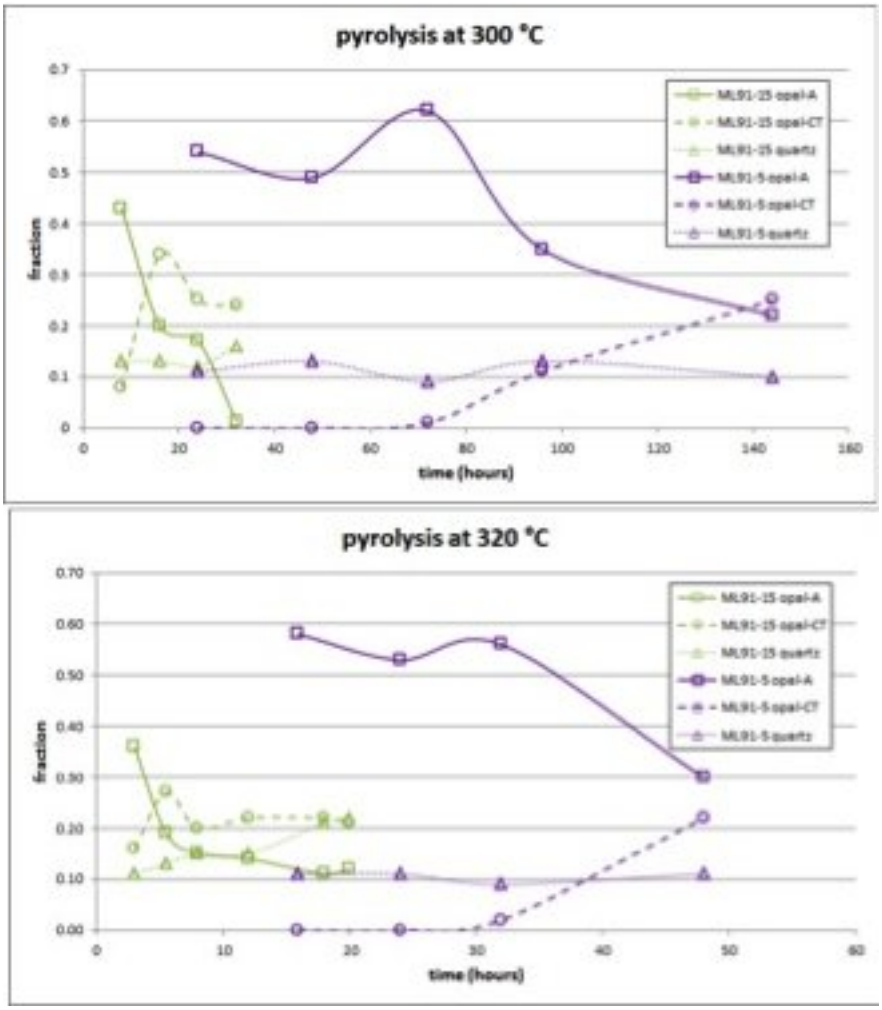

Fig. 2. Approximate sample compositions during pyrolysis at two temperatures. The ML91-15 sample (green) is the low-TOC material; the ML91-5 sample (purple) is the high-TOC material.

References

Dralus, D., 2013, Chemical interactions between silicates and their pore fluids: How they affect rock physics properties from atomic to reservoir scales, PhD thesis, Stanford University, Stanford, CA, 179 p.

Ernst, W.G., and S.E. Calvert, 1969, An experimental study of the recrystallization of porcelanite and its bearing on the origin of some bedded cherts, American Journal of Science, v. 267-A, p. 114 – 133.

Icenhower, J., and P. Dove, 2000, The dissolution kinetics of amorphous silica into sodium chloride solutions: Effects of temperature and ionic strength, Geochimica et Cosmochimica Acta, v. 64, no. 24, p. 4193 – 4203, doi 10.1016/S0016-7037(00)00487-7.

Stein, C. L., and R. J. Kirkpatrick, 1976, Experimental porcelanite recrystallization kinetics: A nucleation and growth model: Journal of Sedimentary Research, v. 46, p. 430 – 435.

BPSM BENCHMARK BASIN MODEL PROJECT

Amrita Sen[1], Tapan Mukerji[2], and Allegra Hosford Scheirer[3]
[1]Department of Geophysics, Stanford University
[2]Department of Energy Resources Engineering, Stanford University
[3]Department of Geological and Environmental Sciences, Stanford University

The BPSM Industrial Affiliates Program incorporates scientists across the School of Earth Sciences. Accordingly, we approach basin and petroleum system models from a variety of perspectives. To complement both the laboratory-based (experimental) approaches to basin modeling and the "observational" approach in which sedimentary basins and their contained petroleum are investigated in 1-D, 2-D, or 3-D, we created a benchmark basin and petroleum system model, also sometimes called a "synthetic" model. The basis for the benchmark model is a set of 24 layers corresponding to actual rock formations from a Cenozoic sedimentary basin. Of the 24 model layers, one is a shale source rock, five are reservoir rocks, and the rest act as overburden rocks, underburden rocks, or seal rocks. To generalize the model, we extracted a rectangular model volume approximately 180 by 100 km in size. Currently the standard model has a grid spacing of 500 m in each of the three coordinate directions, but can be upscaled or downscaled as needed.

The benchmark basin model can be used by the BPSM research group in several ways. First, it can be used as a teaching tool. Professors can prepare labs using the benchmark basin model as a "perfect" data set. Second, it can be used to test the effectiveness and ease of using parameters other than vitrinite reflectance and Tmax for model calibration. Third, it can be used for both scenario testing and workflow testing so that schemes can be developed in a perfect situation before application to the real world environment. Fourth, we can introduce the concept of stochastic descriptions of layer properties rather than the more typical deterministic ones. Finally, we can intersect the field of rock physics with basin and petroleum system modeling in ways that haven't yet been done.

To that end, we would like to start by creating a corresponding seismic volume to go with the basin model and compare this with a version of the model that includes spatial distributions of porosity for the reservoir layers of interest. After simulation, we obtain velocity and density volumes for the model. Based on these, we can obtain a near and far stack seismic volume. The benchmark model provides us both with a base case, as well as an experimental environment in which we can explore the influence of key inputs for basin modeling.

The basin and petroleum system modeling software platform PetroMod allows us to export any properties associated with the benchmark basin model. This is particularly useful because it allows us to bring our simulated scenarios into additional geosciences programs. For this project, there are two such programs of interest: SGems, a Stanford developed geostatistical simulator, and MATLAB, a programming language used by geophysicists to model rock physics and seismic data. As noted above, the scale of the benchmark model is 500 x 500 x 500m. In order to represent the basin at the seismic scale, a more appropriate measurement scale would be on the order of 10 x 10 x 10m. This requires us to downscale our model and provide rock property values. To do this, we can

take advantage of our geostatistics simulator. PetroMod provides us with an average value for the 500 x 500 x 500m grid cells. If, for example, we are working with porosity, we can use a block simulation to preserve the average value calculated by PetroMod. In order to then fill in the 10 x 10 x 10m cells, we can provide a variogram indicating the variation of porosity with regards to distance. This is easily derived from any well log and can be used as an input to our block simulation. In this case, the well log provides us with the variation of porosity with depth.

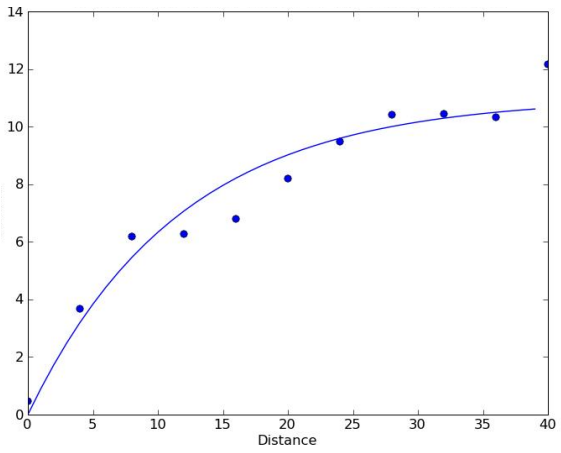

Figure 1. Porosity Variogram derived from well log

A combination of the variogram and "block" data generated by PetroMod allows us to then simulate a downscaled porosity map for our target basin model layer via block simulation. At this point, we can export this downscaled map from SGems and import it into MATLAB.

In order to generate a corresponding seismic volume for the benchmark basin model, we need to populate the model with elastic properties. This can be done, most simply, using a number of rock physics relations. Each basin model layer is associated with a specific lithology; every lithology has a unique mineral bulk modulus. The block simulation provides us with a fine scale porosity map, and PetroMod can provide us with water and oil saturation values when we run a Darcy fluid flow simulation. From this information we can obtain all the properties required to calculate the average bulk modulus of any given cell using the following classical rock physics relations (Gassmann, 1951):

$$K_{Sat} = K_s \frac{\phi K_{Dry} - (1+\phi) K_f K_{Dry} / K_s + K_f}{(1-\phi) K_f + \phi K_s - K_f K_{Dry} / K_s}$$
$$K_{Dry} = K_s \frac{1 - (1-\phi) K_{Sat} / K_s - \phi K_{Sat} / K_f}{1 + \phi - \phi K_s / K_f - K_{Sat} / K_s}, \quad (1)$$

where K_{Sat} and K_{Dry} are the bulk moduli of the rock saturated with the fluid whose bulk modulus is K_f and the rock's dry frame, respectively; K_s is the bulk modulus of the mineral phase; and ϕ is the total porosity of the rock. ϕ is provided by our downscaled map, K_s and K_{Dry} can be obtained from rock physics literature based on laboratory measurements, so

our last missing component to calculate K_{Sat} is K_f.

The K_f, fluid elastic moduli can be determined by simply using a weighted average based on water saturation (S_w), which is used to represent a uniform fluid distribution (Mavko et. al, 2011),

$$K_f = [S_w / K_w + (1 - S_w) / K_g]^{-1} \quad (2)$$

where K_g is the bulk modulus of the saturating hydrocarbon and K_w is the bulk moduli of water.

The elastic moduli can then be directly related to p-wave and s-wave velocity. At this point we can also create a corresponding seismic volume using a number of pre-existing MATLAB functions. To summarize, we can represent this workflow with the following diagram.

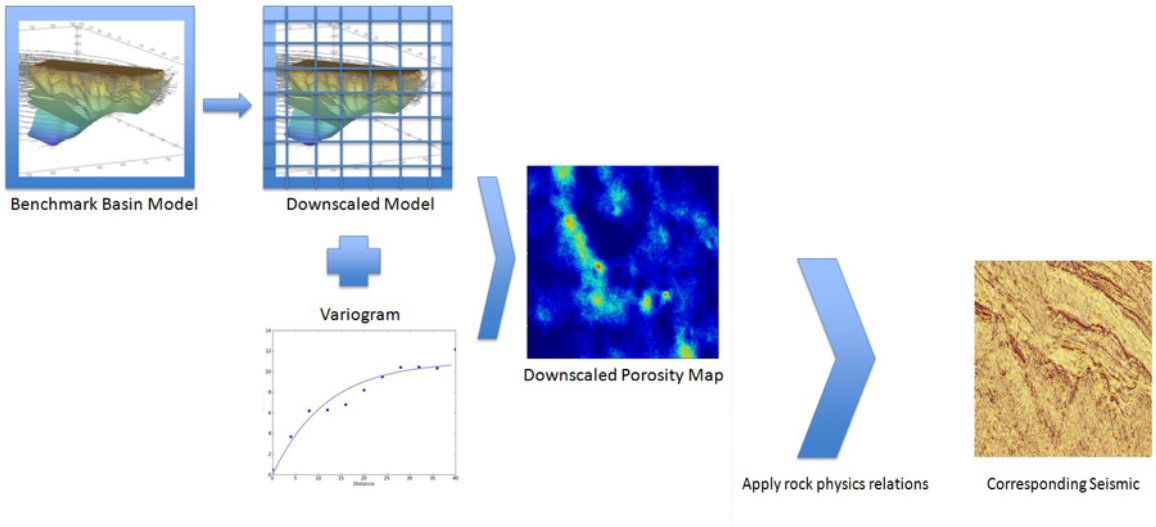

Figure 2. Benchmark Basin Model to Seismic Volume Workflow

The process described above provides us with a workflow that integrates basin modeling, geostatistics, and geophysics. This can be particularly useful for a number of industry related processes such as updating seismic based on basin modeling, or vice versa—updating a pre-existing basin model based on reservoir seismic surveys. In addition, the incorporation of a geostatistics simulator gives us the ability to downscale our basin model and incorporate reservoir and well log scale data into our calculations. This gives us the ability to essentially create a number of possible geologic scenarios with fine-scale details that can still represent the average answer provided by the basin model. In real world applications, seismic is not available across the entire basin, so this workflow allows us to estimate the details between seismic surveys taken across specific points in a basin, such as producing reservoirs. Taking our model to the next step and generating a seismic volume also has the potential to allow us to create 4D models based on current field production, which is a topic that has recently gained popularity and has not yet been explored in an integrated method involving basin modeling.

We would like to acknowledge Ken Peters, Carolyn Lampe, and Les Magoon for their discussions, suggestions and input on this project.

REFERENCES

Gassman, F., 1951, Uber die Elastizitat poroser Medien: *Vier. Der Natur. Gesellschaft Zurich,* 96, 1-23.

Mavko, G., T. Mukerji, and J. Dvorkin, 2009, The Rock Physics Handbook: Cambridge University Press, 522 pp.

A GEOCHEMICAL ASSESSMENT OF THE UTICA SHALE IN THE MOHAWK VALLEY OF NEW YORK

Will Thompson-Butler and Francis Macdonald[1]
Department of Geological and Environmental Sciences, Stanford University (formerly Harvard University)
[1]Harvard University

Deposited in the Taconic foredeep during the late Ordovician, the Utica Shale has garnered significant attention as a potential unconventional resource play in the eastern United States. The primary goal of this project was to take advantage of nearby outcrops in order to perform a carbon isotope analysis on a complete vertical section of the Utica and to employ this analysis towards observations of the environment and style of deposition for the unit. 78 shale samples were taken from the lower Flat Creek Member of the Utica Shale while 44 were taken from the upper Indian Castle Member, both at almost 1 m resolution. Carbonate samples from the intermediate Dolgeville Formation and underlying Trenton Group as well as bentonite samples from throughout the sample area were also taken, however carbon isotopes became the main emphasis of the study.

The primary outcomes of this analysis were evidence for diachronous deposition of the Utica Shale across the state of New York as well as suggestions for appropriate future work as the project moves forward. In addition, TOC values for the Flat Creek Member appear consistently higher than those of the Indian Castle Member (1-3.5% versus about 0.5-2%). This seems to coincide with a positive trend in carbon isotope values, including what I believe is a section of the Guttenberg Isotopic Carbon Excursion (GICE) in the basal 30 m of the Flat Creek Member. Exploring these trends and their relationship to the depositional setting of the Utica Shale could carry ramifications for the Utica as a source rock and potential unconventional resource. Initial future work would include data corroboration from further vertical sections as well as integration of radiometric data from CA-ID-TIMS on bentonite bed zircons. The figures below illustrate the project sample locations, a full stratigraphic section for the measured area, and a graph depicting the organic and inorganic carbon isotopes as well as the TOC values for the lower Flat Creek section.

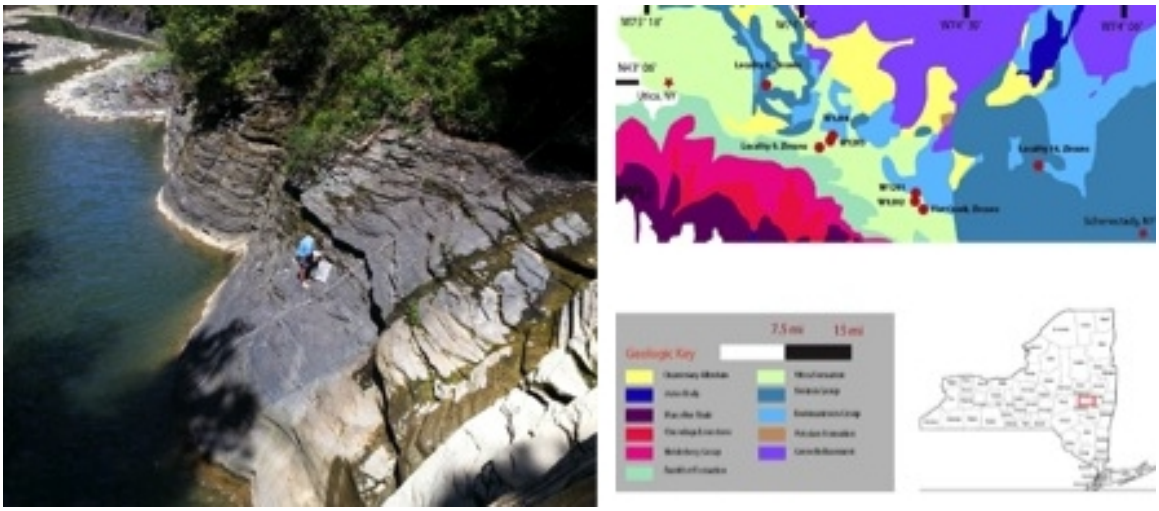

Figure 1. (l) A section of the Flat Creek Member of the Utica Shale with my thesis advisor for scale. The recessive bed indicates one of the bentonite sample localities; (r) A geologic map depicting the locations of sampled sections in the Mohawk Valley, New York.

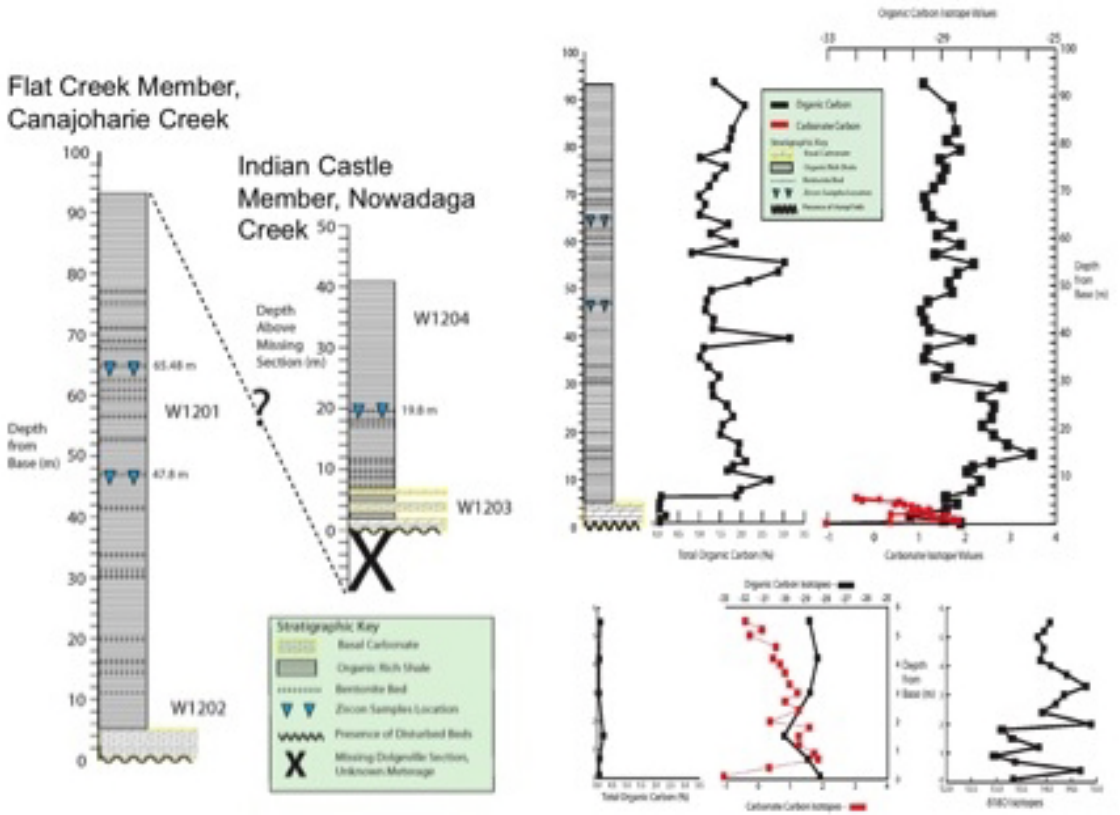

Figure 2. (l) A stratigraphic section for the sampled Utica area; (r) Results for the flat creek section depicting TOC and organic carbon isotopes in the top section and TOC, inorganic carbon isotopes and oxygen isotopes for the carbonate rich Utica base in the bottom section.

CHARACTERIZATION AND SPATIAL UNCERTAINTY QUANTIFICATION FOR UNCONVENTIONAL GAS RESOURCES IN PICEANCE BASIN, COLORADO

Yao Tong[1], Allegra Hosford Scheirer[2], Tapan Mukerji[1]
[1]Department of Energy Resources Engineering, Stanford University
[2]Department of Geological and Environmental Sciences, Stanford University

With rising energy demand and depletion of conventional resources, exploration and development of unconventional resources have become increasingly important. Gas shale and tight gas represent an enormous potential among the unconventional resources. Our study area—Piceance Basin, Colorado—contains tremendous gas reserves in place, and it is important to understand the different factors that can affect the generation and accumulation of the gas resources. This abstract summarizes an ongoing interdisciplinary study for quantitatively modeling unconventional gas resources in the Piceance Basin and in particular, the use of geostatistical approaches to address spatial uncertainties, which are rarely tackled in basin and petroleum system modeling discipline.

Quantifying spatial uncertainties using geostatistical approach and stochastic workflow

The integrated nature of basin modeling requires incorporating parameters that cover a large spatial and temporal interval and are often associated with uncertainties. With one deterministic basin model, though it typically represents the best estimate scenario based on known knowledge, it is not sufficient to characterize the associated uncertainties of the complex process. Previous uncertainty quantification work in this discipline has focused mainly on traditional Monte Carlo techniques with parameter uncertainties. Jia et al. (2012) pointed out that spatial uncertainties can have an equally strong impact on the output as parameter uncertainties. To better quantify the complex associated uncertainties in basin models, specifically spatial uncertainties, we propose a stochastic modeling approach in which multiple realizations of spatial uncertain parameters will first be generated using geostatistical tools SGeMS (Stanford Geostatistical Modeling Software), then an ensemble of basin models corresponding to these realizations can be constructed and simulated. In comparison to the traditional single deterministic basin model approach, this stochastic workflow provides a new way of tackling spatial uncertainties that will ultimately assist in risk assessment in this discipline. The workflow is demonstrated in the following Figure 1.

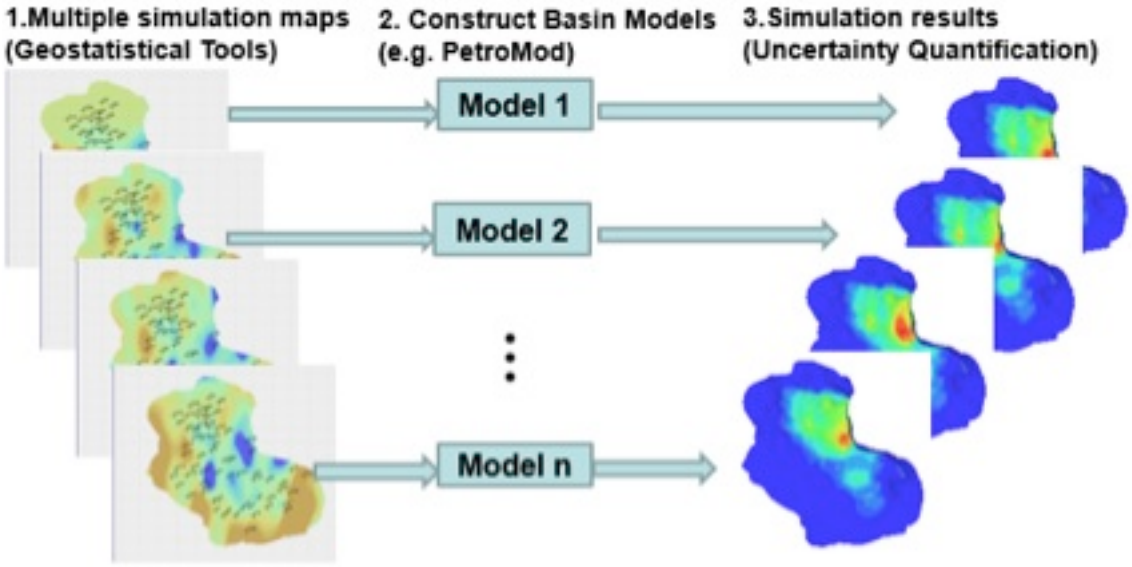

Figure 1. Stochastic workflow based on geostatistical tools and multiple basin models.

Example of stochastic basin model workflow application

The proposed stochastic modeling approach and geostatistical tool application is implemented to improve the characterization of the source rock thickness. The regional geological study shows that the primary source rock 'Cameo Coal' refers to the coal-prone coastal-plain section in the sequence between Rollins Member (shoreline sandstone) and the next higher marine transgression. Though it is often described as 'wide-spread thick coal', basin-wide coal thickness determinations remain uncertain. A typical approach would be to create a uniform thickness map where each grid point is equal to the average coal thickness value; another approach is a map created from interpolation (by inverse distance, Laplace's method or kriging) between known coal thicknesses at discrete well locations. These approaches largely underestimate the spatial uncertainty in the source rock distribution, especially when the hard data are sparse. Accordingly, multiple realizations from stochastic simulation algorithm are introduced in this workflow. In the stochastic workflow, multiple realizations of coal thickness maps are generated using Sequential Gaussian Simulation algorithm. Figure 2 shows one smooth estimation map with three realizations of coal thickness maps generated from stochastic simulation. All of them honor the 67 well data equally well but result in varying spatial patterns of coal thickness.

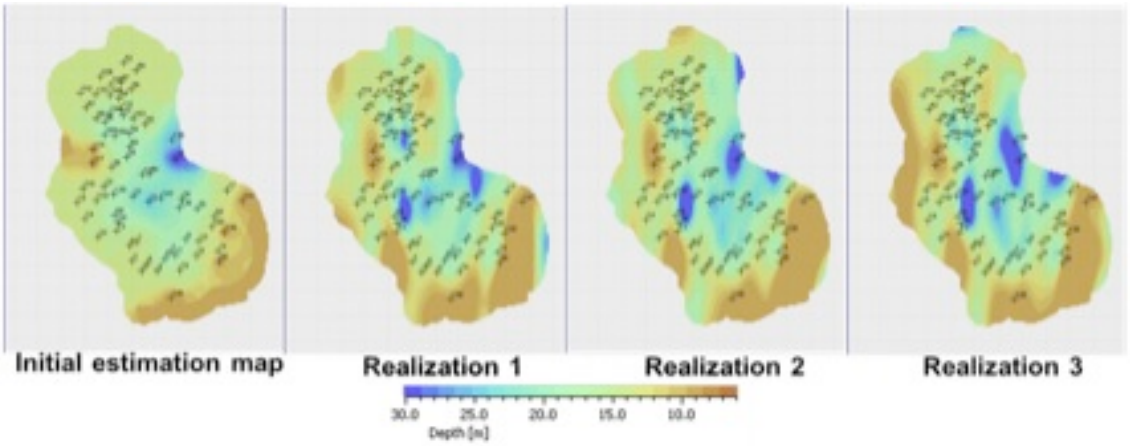

Figure 2. Multiple source rock thickness maps generated using Sequential Gaussian.

The simulation maps are generated from a Gaussian variogram with a maximum range of 50 grid blocks; this was selected based on the assumption of a smooth spatial variation feature of the coal. We use 67 coal thickness determinations as "hard data" to represent a sparse data scenario where the uncertainty is large.

The randomness introduced by the stochastic simulation method represents the large uncertainties of our knowledge. Notice that the idea of utilizing stochastic simulation is not to provide the best single estimation but rather to create multiple, equally-probable realizations so that we can utilize this ensemble and obtain predictions with an associated uncertainty range. In this case, the uncertainties of the spatial variation of the source rock thickness are first captured in these realization maps and then incorporated into the basin models. Thus, 4 basin models were built and simulated based on these 4 different source rock thickness scenarios while keeping all other model input the same. The model predictions of gas generation at present day are given in the table below. The uncertainty range in these predictions shows the impact of spatial uncertainties in source rock thickness when data are limited.

	Initial Model	Basin Model 1	Basin Model 2	Basin Model 3
Source Rock Thickness	Estimation map	Source rock realization 1	Source rock realization 2	Source rock realization 3
Total Gas [Tcf]	19.36	17.82	20.47	22.09
Difference	0	-8%	+6%	+14%

PETROLEUM GENERATION KINETICS: SINGLE- VERSUS MULTIPLE HEATING-RATE OPEN-SYSTEM PYROLYSIS

K.E. Peters[1,2] and A.K. Burnham[3]
[1]Schlumberger Information Solutions, Mill Valley, CA 94941; kpeters2@slb.com
[2]Department of Geological and Environmental Sciences, Stanford University
[3]American Shale Oil Corporation, LLC, Livermore, CA 94550; akburnham@comcast.net

Waples et al. (2002, 2010) and Waples and Nowaczewski (2014) promote one-run, open-system pyrolysis using a single heating rate (ramp) to determine the petroleum generation kinetics of source rock samples because they are faster, less expensive, and presumably yield results similar to those from multiple-ramp experiments. They maintain that the key to single-ramp kinetics is to use a fixed frequency factor (A = 1 or 2 x 10^{14} sec^{-1}), which constrains non-unique activation energy (E_a) distributions to a single geologically reasonable result. The purpose of this paper is to compare the reliability of various combinations of open-system pyrolysis heating rates to determine the kinetics of petroleum generation from source rocks.

The data show that although some one-ramp pyrolysis experiments yield results similar to those from multiple-ramp experiments, one-ramp kinetics are generally unreliable. Kinetic results based on three pyrolysis temperature ramps closely approximate those from six runs, provided that the three ramps span an appropriate range. Ramps of 30 and 50°C/min are generally too fast to obtain a good kinetic fit using Pyromat II® data due to delayed heat transfer between the sample and thermocouple. Therefore, at least three pyrolysis ramps are recommended that span a ten-fold variation of slow rates, such as 1, 3, and 10°C/min or 1, 3, 5, and 10°C/min. Replicate analyses are best, particularly for the highest and lowest heating rates because they dominate the calculated kinetic results.

Fifty-three worldwide source rock samples (Peters et al., 2006) span kerogen types I, II, IIS, II/III, and III and are immature to slightly mature with respect to oil generation. Ground aliquots (<60 mesh, ~10 mg) of whole rock were subjected to Pyromat II® open-system micropyrolysis at one or more of the following rates: 1, 3, 5, 10, 30, and 50°C/min. Continuous temperatures were measured during pyrolysis using a calibrated thermocouple in direct contact with the sample. Products were transferred to a flame ionization detector by helium flow at 50 ml/min. Pyrolyzate peaks were processed using Kinetics05® software to derive chemical kinetic rate models (Burnham and Braun, 1999). The calculations assume that thermal alteration of kerogen in source rock proceeds as a collection of parallel first-order reactions as described by the Arrhenius equation.

To test the variability of kinetic models derived from a single pyrolysis heating rate, one sample was analyzed 16 times. Data from the 30ºC/min pyrolyses were used for single-run models because that rate is most similar to Rock-Eval pyrolysis (25°C/min). The 16 single-run kinetic models with fixed A (1 x 10^{14} sec^{-1}) show a mean E_a of 53.54 ± 0.28 kcal/mol. Assuming 3ºC/my, the temperature range at 10, 50, and 90% transformation ratio (TR) is 9.8 ± 2.3, 2.6 ± 0.8, and 7.8 ± 2.2°C, respectively. This is the minimum error for single-run analyses conducted using Pyromat II.

Comparison of kinetic models derived from single and multiple heating rates for the 53-sample suite shows that the impact of fixing the frequency factor is offset by adjustment of the mean of the activation energy distribution in the Kinetics05 optimization (Fig. 1). The correlation ($R^2 > 0.99$) holds for all kerogen types. Multiple pyrolysis heating ramps are needed to determine the best A value, whereas the pyrolysis peak shape determines the E_a distribution and T_{max} determines the mean E_a. When the data quality is good, using a fixed A value allows reasonable calculations of the E_a distribution. Good programmed pyrolysis data show uniform peak shape and T_{max} increases linearly with the log of the heating rate (Kissinger, 1957). In such a case, single and multiple run kinetic models yield similar results. However, when geologic heating rates are applied to these models, differences between them are magnified. Assuming 3°C/my, the single-run kinetic models yield temperatures at 50% TR ranging from 17°C higher to 10°C lower than those from multiple kinetic models with optimized A values (Fig. 2). These variations do not correlate with kerogen type, so knowledge of kerogen type cannot be used to adjust the single-run kinetics in a consistent manner.

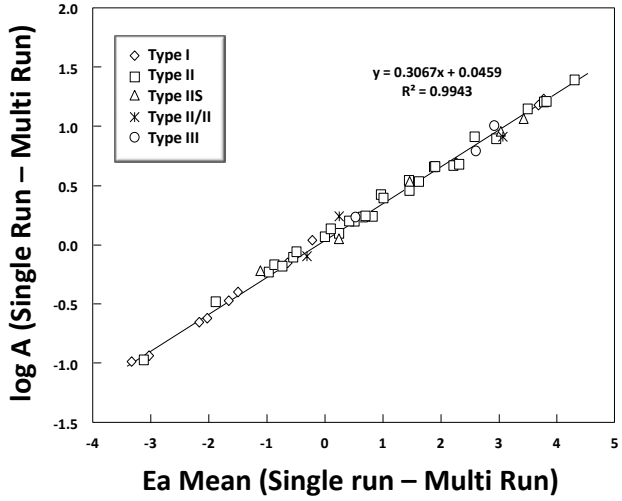

Figure 1. Comparison of kinetic models derived from single (30°C/min) and multiple pyrolysis heating rates (1, 3, 5, 10, 30, 50°C/min) for 53 worldwide source rock samples shows that the impact of fixing the frequency factor in a single ramp experiment is effectively offset by adjustments of the mean activation energy distribution in the multiple ramp experiments, regardless of kerogen type.

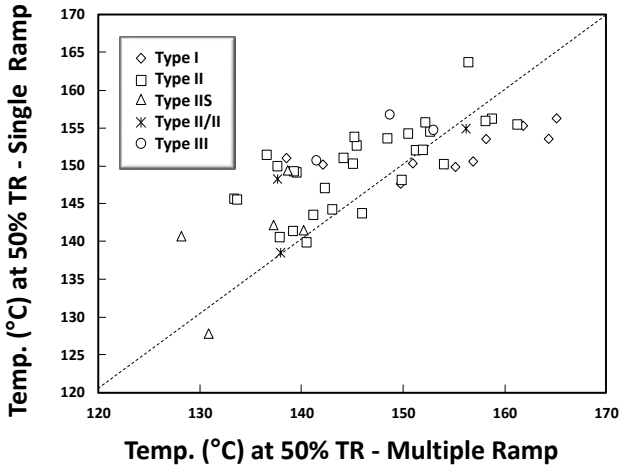

Figure 2. Assuming 3°C/my, single-run kinetic models with fixed *A* (1 x 10^{14} sec^{-1}) yield calculated temperatures at 50% transformation ratio (TR) ranging from 17°C higher to 10°C lower than those from multiple kinetic models with optimized *A* (combinations of 1, 3, 5, 10, 30, 50°C/min ramps).

Samples from the Kimmeridge Clay and Monterey formations (type II and IIS kerogen, respectively) are used as examples. The Kimmeridge sample yields an optimized *A* (1.28 x 10^{14} sec^{-1}) close to that recommended by Waples et al. (2002, 2010) for the single run models, while the optimized *A* for the Monterey is significantly lower (1.13 x 10^{13} sec^{-1}). Figs. 3-4 show calculated temperatures at 10, 50, and 90% TR in the samples based on Kinetics05 optimized distributed reactivity models using various combinations of Pyromat II heating rates (1, 3, 5, 10, 30, and 50°C/min). The number of ramps in the figures (left) range from one to six and selected combinations of ramps are labeled. For example, the six ramp experiment is labeled "1,3,5,10,30,50". The ramp range in the figures (right) is the difference between the maximum and minimum ramp for each experiment. For example, a ramp range of 49°C/min corresponds to ten different temperature ramp combinations.

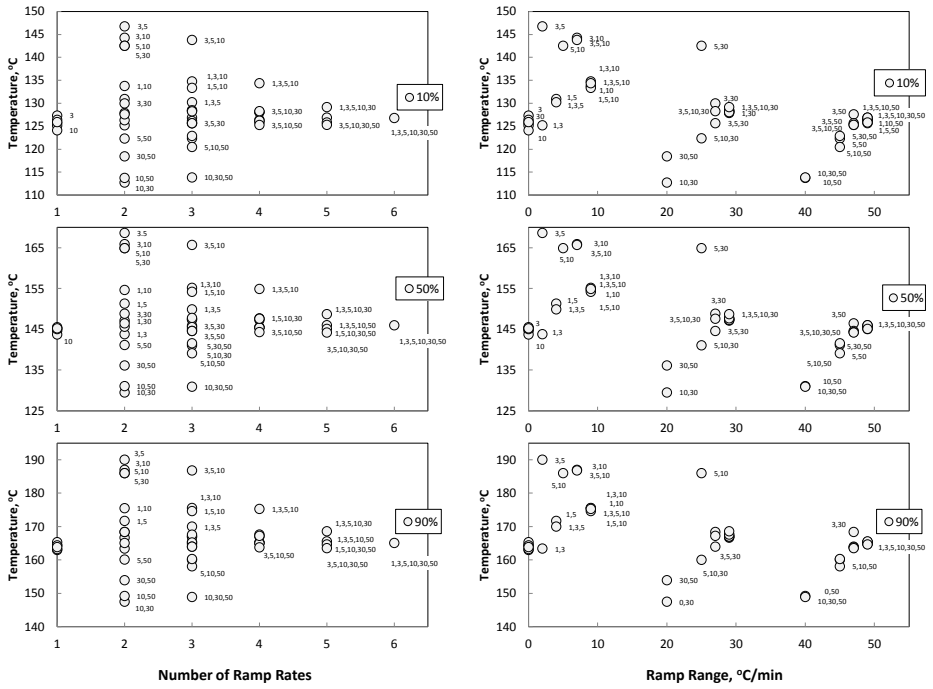

Figure 3. Kinetics05 optimized temperatures at 10, 50, and 90% transformation ratio (TR) using various combinations of Pyromat II heating rates (1, 3, 5, 10, 30, and 50°C/min) for the Kimmeridge Clay sample. Ramp range is the difference between the maximum and minimum ramps.

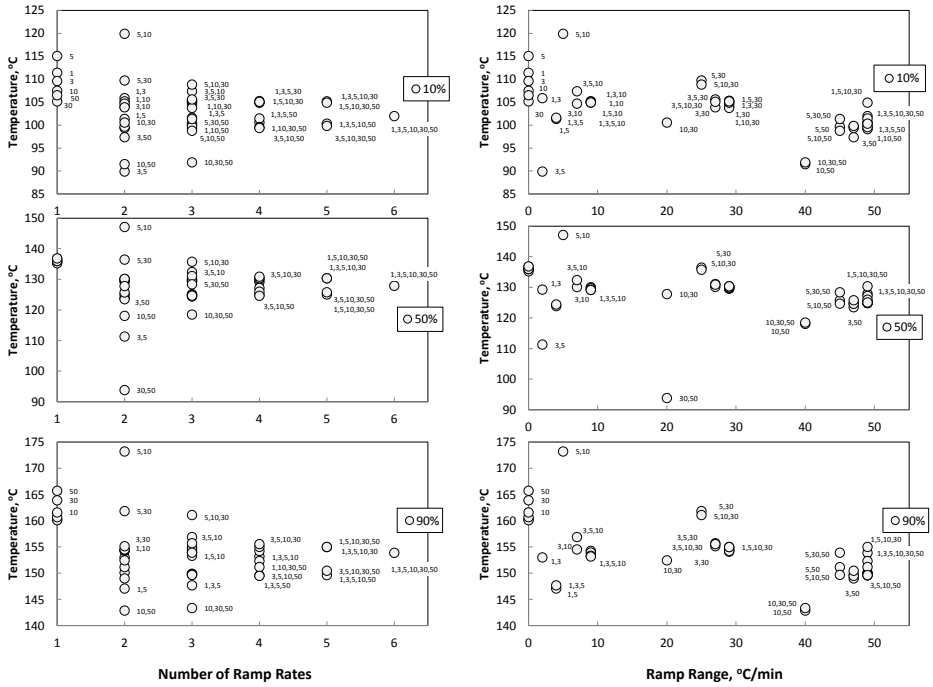

Figure 4. Kinetics05 optimized temperatures at 10, 50, and 90% transformation ratio (TR) using various combinations of Pyromat II heating rates (1, 3, 5, 10, 30, and 50°C/min) for

the Monterey sample. Ramp range is the difference between the maximum and minimum ramps.

Six single-ramp pyrolysis experiments with fixed *A* (1×10^{14} sec^{-1}) for the Kimmeridge sample at 1, 3, 5, 10, 30, and 50°C/min (number of ramps, n = 1; Fig. 3) show narrow ranges of calculated temperature at 10, 50, and 90% TR (124.1-127.3°, 143.7-145.5°, and 163.0-165.3°C, respectively). These single-ramp predictions correspond reasonably well with those based on a six-ramp experiment with free *A* (n = 6; Fig. 3) in which calculated temperatures at 10, 50, and 90% TR are 126.8°, 146.0°, and 165.1°C, respectively. If other ramps were not considered (e.g., two-, three-, four-, and five-ramp experiments), then one might conclude that temperatures calculated from a single-ramp Kimmeridge pyrolysis experiment at 10, 50, and 90% TR are as reliable as those based on a six-ramp experiment.

However, the data show that multiple-ramp experiments are more precise than those based on single ramps. Figs. 3-4 (left) show that scatter in predicted temperature decreases from two- to six-ramp experiments. Optimized temperatures at 10, 50, and 90% TR for the Kimmeridge sample using combinations of two, three, four, five, and six ramps show wide scatter that decreases with increasing number of ramps. For example, two-ramp Kimmeridge experiments (n = 2; Fig. 3) include fifteen combinations of Pyromat II experiments: 1,3; 1,5; 1,10; 1,30; 1,50; 3,5; 3,10; 3,30; 3,50; 5,10; 5,30; 5,50; 10,30; 10,50; and 30,50°C/min. The experiments show a wide range of calculated temperatures at 10% TR (34.03°C), which decreases from three- to four- to five- to six-ramp experiments (30.0°C, 9.1°C, 3.9°C, and 0°C, respectively). This suggests that similar calculated temperatures for the single- and six-ramp Kimmeridge experiments are fortuitous. One might assume that six-ramp runs yield the most reliable temperatures. However, evidence suggests that more reliable temperature predictions are achieved by excluding faster ramps (e.g., 50°C/min), as discussed below.

The data for the Monterey sample also indicate that more ramps result in more precise temperature determinations at 10, 50, and 90% TR. However, calculated temperatures for single-ramp Monterey experiments are unlike those for the six-ramp experiment (Fig. 4), which shows that single-run kinetic parameters are not reliable for all samples. Six single-ramp experiments on Monterey samples at 1, 3, 5, 10, 30, and 50°C/min (n = 1; Fig. 4) show various ranges of calculated temperature at 10%, 50%, and 90% TR (105.2-115.0°, 135.3-136.9°C, and 160.1-165.7°C, respectively). These single-ramp predictions differ from those based on six ramps (n = 6; Fig. 3), in which calculated temperatures at 10%, 50%, and 90% TR are 102.0°, 127.9°, and 153.9°C. Like the Kimmeridge data, the Monterey data show that more ramps yield more precise calculated temperatures at 10, 50, and 90% TR.

The most precise Kinetics05 temperature predictions are obtained when pyrolysis ramps span a wide range (Figs. 3-4, left). However, fast ramps such as 50°C/min are best excluded, as indicated by the ramp range in the figures (right). Single-ramp experiments have ramp range of zero. Labels in Figs. 3-4 (right) show that in general, lower temperatures are predicted for ramp ranges that include 30 and 50°C/min heating rates

(lower portion of each figure), while higher temperatures are predicted for ramp ranges that exclude them. In particular, the 50°C ramp appears to be too fast to allow equilibration and the thermocouple temperature at any time may be lower than that in the rock.

References

Burnham, A.K. and Braun, R.L. [1999] Global kinetic analysis of complex materials: Energy & Fuels, **13**, 1-22.

Kissinger, H.E. [1957] Reaction kinetics in differential thermal analysis: Analytical Chemistry, **29**, 1702-1706.

Peters, K.E., Walters, C.C. and Mankiewicz, P.J. [2006] Evaluation of kinetic uncertainty in numerical models of petroleum generation: American Association of Petroleum Geologists Bulletin **90**, 1-19.

Waples, D.W. and Nowaczewski, V.S. [2014] Source-rock kinetics. In Encyclopedia of Petroleum Geoscience, New York, Springer, http://siriusdummy.files.wordpress.com/2013/11/perspective-on-sr-kinetics-ss.pdf

Waples, D.W., Vera, A. and Pacheco, J. [2002] A new method for kinetic analysis of source rocks: development and application as a thermal and organic facies indicator in the Tithonian of the Gulf of Campeche, Mexico. 8th Latin American Congress on Organic Geochemistry, Cartagena, Abstract, 296-298.

Waples, D.W., Leonard, J.E., Coskey, R. Safwat, S. and Nagdy, R. [2010] A new method for obtaining personalized kinetics from archived Rock-Eval data, applied to the Bakken Formation, Williston Basin. American Association of Petroleum Geologists Annual Convention, Calgary, Abstract #90108.